OPTICA

Limits and prospects for long-baseline optical fiber interferometry

CHRISTOPHER HILWEG,[1,2,†,*] DANIAL SHADMANY,[3,4,†] PHILIP WALTHER,[1] NERGIS MAVALVALA,[5] AND VIVISHEK SUDHIR[5,6,7]

[1]*University of Vienna, Research Network for Quantum Aspects of Space Time (TURIS), Boltzmanngasse 5, 1090 Vienna, Austria*
[2]*Institute for Quantum Optics and Quantum Information (IQOQI Vienna) of the Austrian Academy of Sciences, Boltzmanngasse 3, A-1090, Vienna, Austria*
[3]*The James Franck Institute and Department of Physics, University of Chicago, Chicago, Illinois 60637, USA*
[4]*Department of Physics, Stanford University, Stanford, California 94305, USA*
[5]*LIGO Laboratory, Massachusetts Institute of Technology, Cambridge, Massachusetts 02139, USA*
[6]*Department of Mechanical Engineering, Massachusetts Institute of Technology, Cambridge, Massachusetts 02139, USA*
[7]*e-mail: vivishek@mit.edu*
**Corresponding author: christopher.hilweg@univie.ac.at*

Today's most precise optical instruments—gravitational-wave interferometers and optical atomic clocks—rely on long storage times for photons to realize their exquisite sensitivity. Optical fiber technology is the most widely deployed platform for realizing long-distance optical propagation. Yet, its application to precision optical measurements is sparse. We review the state of the art in the noise performance of conventional (solid-core) optical fibers from the perspective of precision optical measurements and quantum technology that rely on precise transfer of information over long distances. In doing so, we highlight the limitations of this platform and point to the opportunities that structured fiber technology offers to overcome some of these limitations.

1. INTRODUCTION

An ancient material—sand—underlies much of the technological prowess of the modern world. In particular, the information age that we live in is enabled by the fact that ultra-pure fused silica can sustain ultra-low-loss optical propagation [1,2]. A century-long pursuit in ceramic science and glass technology [3–6], together with theoretical understanding of optical loss mechanisms in these materials [1,7], has resulted in optical fibers limited only by intrinsic losses as low as ≈ 0.14 dB/km (at a wavelength of 1.55 μm) [8]. Together with the laser, low-loss optical fibers enable the delivery of highly coherent radiation across large distances.

Indeed, optical loss is a convenient figure of merit to gauge the maturity of an optical technology and a relevant one for its application in both classical and quantum technologies. Today's most precise measurements—incidentally, of space [9,10] and time [11,12], at a precision around one part in 10^{20}—are carried out using ultra-low-loss optical interferometers. Low loss in these interferometers leads to less optical quantum noise thereby improving their sensitivity [13]. In optical quantum networks the effect of loss is two-fold: loss of photons that carry quantum information and/or losses in the classical communication channel required to complete a quantum communication protocol both limit the fidelity of communication [14]. In both cases, reduction of losses and extraneous noise are central to the scientific goals they serve.

On one hand, state-of-the-art free-space Fabry–Perot interferometers—such as the ones employed in Advanced LIGO or as references in optical atomic clocks—realize losses as low as ≈ 10 ppm/km [15], which is apparently three orders of magnitude lower than the state-of-the-art loss of contemporary solid-core optical fibers [8,16]. This is possible since photons interact only occasionally with lossy mirror surfaces. On the other hand, losses in the few-micrometer-thick mirror coatings of interferometer cavities can be as large as several tens of dB/km, orders of magnitude worse than the pristine fused silica core of an optical fiber.

In an optical fiber, precisely because the optical field lives in a medium, physical processes in the medium induce optical noises and nonlinearities that preclude the use of high powers to overcome the limitations posed by the already miniscule losses. It is in this context that structured optical fibers seem to offer a unique opportunity: structuring of the core offers a new degree of freedom that allows independent engineering of optical noises and losses. In fact, just last year, a structured fiber with loss comparable to a solid core was demonstrated [17]. Figure 1 depicts the dramatic progress in the reduction of optical loss achieved in structured fibers in recent years, while solid-core fiber technology seems to be limited by 40 years of incremental improvement. Thus, the
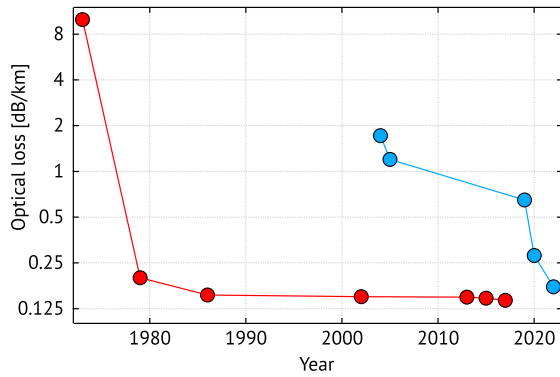
Fig. 1. Evolution of fiber attenuation for solid- (red) and hollow-core fibers (blue) for wavelengths in the telecom C-band (lines to guide the eye). Solid-core fibers improved from about 10 dB/km (1973) [18], 0.2 dB/km (1979) [19], 0.154 dB/km (1986) [20], 0.15 dB/km (2002) [21], 0.149 dB/km (2013) [22], and 0.1467 dB/km (2015) [23] to finally 0.1419 dB/km (2017) [8,16]. Initial losses in hollow-core photonic bandgap fibers (HC-PBGF) of 1.72 dB/km (2004) [24] and 1.2 dB/km (2005) [25] were significantly reduced over the last years by use of nested antiresonant nodeless fibers (NANF) down to 0.65 dB/km (2019) [26], 0.28 dB/km (2020) [27], and even 0.174 dB/km (2022) [17]. While for solid-core fibers, the improvements slowly converge towards the theoretical minimum governed by Rayleigh scattering, HCFs and in particular antiresonant fibers show rapid development and might surpass solid core fibers in the near future.

question of whether optical fiber technology, given its mature state, can supplant or supplement the conventional platforms employed in precision and quantum measurements needs a fresh appraisal.

We first review the primary limitations of solid-core optical fibers as it pertains to applications in precision optical sensing, including the effect of optical noises and nonlinearities. We then discuss the state of knowledge of these same factors in structured optical fibers, and highlight opportunities for further research into their properties. Given the obvious practical advantage of optical fibers over free-space optical links—immunity to electromagnetic interference, single-mode performance, and ease of deployment— we expect that a careful study of the optical noise properties of structured fibers may renew interest in the application of optical fibers to precision quantum sensing and communication.

To quantify the performance of large optical fiber interferometers, and ultimately be able to compare them to their free-space counterparts, a simple Mach–Zehnder interferometer (MZI) is considered (Section 2). We work out all known relevant sources of intrinsic noise in an optical fiber that can affect the performance of such an interferometer. In particular, we review a panoply of noises intrinsic to optical fibers (Section 3) including scattering processes, thermodynamic noises, and noises due to nonlinear optical processes. We then briefly survey the major extrinsic sources of noise (Section 4) that affect all fiber interferometers, including environmental perturbations and noise arising from the input optical field. The results we derive for this concrete example can be easily transferred to other topologies and applications that rely on phase coherence.

2. OPTICAL FIBER MACH–ZEHNDER INTERFEROMETER

We consider the MZI shown in Fig. 2: a fiber coupler (FC) splits the incoming light field—prepared in a pure polarization state

of the form $\mathbf{E}(t) = \mathbf{p}_0 E_0 \exp(i\omega_0 t)$, with unit polarization $\mathbf{p}_0$, amplitude E_0, and angular frequency ω_0—into two branches of lengths L_1 and L_2 before they are recombined at a second FC. This simple choice already discounts the spatial mode of the field, whose potential distortions in the fiber are not of interest to us. The outputs of the second FC are directed to a pair of photosensitive detectors whose output photocurrents are subtracted and recorded. To consider the possibility of heterodyne detection, one of the arms of the interferometer carries an ideal modulator, which shifts the frequency of light in that arm by ω_h.

It can be shown [see Supplement 1] that the optical power falling on the two detectors A/B is

$$P_{A,B}(t) = P_0 R_{A,B}(1 \pm V_{A,B} \cos \eta \cos[\omega_h t + \phi(t)]), \qquad (1)$$

where $P_0 \propto |E_0|^2$ is the power sent into the interferometer. The splitting ratios of the two FCs and the losses along each arm are captured by $R_{A,B}$, describing the transmissivity of each arm of the interferometer, and $V_{A,B}$, which is the ideal (perfect polarization overlap) interference visibility as measured by detectors A/B. Note that in general, $R_A \neq R_B$ and $V_A \neq V_B$. The angle between the polarization states of light (in the Poincaré sphere, see Supplement 1) before they enter the combining FC is given by 2η, while $\phi(t) = \bar{\phi} + \delta\phi(t)$ is the phase difference between the two arms, consisting of a mean phase offset $\bar{\phi}$—possibly due to a length mismatch between the two arms—and a fluctuating phase $\delta\phi$— consisting of the signal of interest, riding atop extraneous phase fluctuations from the interferometer. The difference photocurrent ultimately recorded is proportional to $P_A - P_B$. Thus, Eq. (1) suggests that noise in the photocurrent is primarily due to apparent fluctuations in the phase, polarization, and optical power in the interferometer.

The precise manner in which these fluctuations are transduced into the photocurrent depends on how the signal phase is extracted [28–34]. The simplest and most sensitive is active homodyne demodulation where the interferometer is maintained at quadrature (i.e., $\bar{\phi} = \pi/2$) using a feedback loop. For an interferometer with a large difference in the mean length between the two arms, this can be most easily achieved by controlling the laser frequency, while for a nearly balanced interferometer, by controlling the residual length difference. In either case, depending on the relative ratio of the extraneous noise in the phase quadrature and environmental noise that drives the interferometer away from the phase quadrature, the choice of gain of the feedback loop to stabilize the interferometer will dictate where the signal of interest is best extracted from. In the high-gain regime—necessary when environment noise tends to destabilize the interferometer, and there is no separation in frequency between the signal and extraneous noise—the signal is best extracted from inside the feedback loop. In the complementary low-gain regime, the signal can be extracted from outside the feedback loop [35]. In heterodyne readout [32], the signal can be upconverted to frequencies around the heterodyne local oscillator, thereby producing a convenient frequency separation between the phase fluctuations and electronic noise from the photodetection process. The price to pay is that additional quantum noise in heterodyne readout makes it at least 3 dB less sensitive than homodyne readout [36,37].

In the ideal case of (balanced) homodyne detection, all noise that obfuscates a phase signal of interest arises from various physical processes intrinsic to the optical fiber that produces apparent phase and polarization noise. In the following, we tour the zoo of
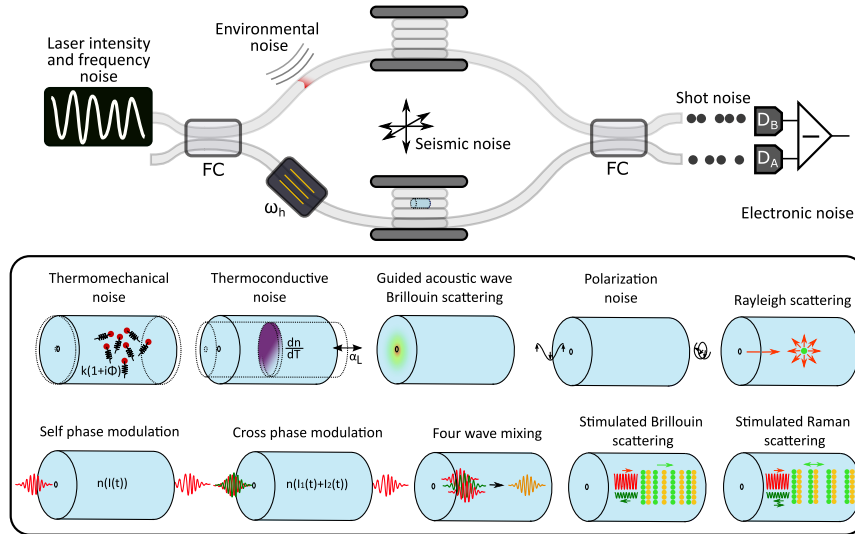
Fig. 2. Top panel shows a schematic fiber Mach–Zehnder interferometer probed by a noisy laser and perturbed by environmental noises (see Section 4). In addition to these extrinsic sources of noise that affect the interferometer, the optical fiber is itself a source of a panoply of noises, depicted schematically in the bottom panel (Section 3). The most important linear sources of intrinsic noise are shown in the first row and discussed in Section 3.A, while we break down the nonlinear noise terms, shown in the second row, in Section 3.B. Thermodynamic phase noise, arising from a combination of mechanical and thermal dissipation, is one of the main limitations in optical fiber interferometry and is especially important for long fibers at low ($\lesssim 1$ kHz) Fourier frequencies (Section 3.A.2). In addition, elastic scattering of light by transverse acoustic modes in the fiber, an effect known as guided acoustic-wave Brillouin scattering (GAWBS), leads to a very complex phase noise spectrum with resonances occurring already in the low MHz range and a behavior at low frequencies that is not yet fully understood. Polarization noise in a fiber interferometer arises from birefringence fluctuations in either the fiber itself or the fiber connection to the laser (Section 3.A.3). Rayleigh scattering, where light scatters off static density variations frozen into the fiber, becomes an important source of noise for narrow-linewidth lasers (Section 3.A.1). For high input powers, nonlinear scattering effects, such as self- and cross-phase modulation (SPM/XPM), add phase noise to the output signal, where the latter occurs only if multiple wavelengths are multiplexed into the fiber. Four-wave mixing (FWM) is also of particular importance for wavelength division multiplexing applications and introduces power losses depending on the phase matching between the involved light fields. Finally, the inelastic scattering of photons from acoustic (stimulated Brillouin scattering, SBS) or optical (stimulated Raman scattering, SRS) phonons restricts the transmittable power through an interferometer, where the former is the dominant source of nonlinear power loss (Section 3.B).

such noises. These include linear noise sources (Section 3.A)—where the propagating optical field does not change the material properties of the fiber—and nonlinear noise sources (Section 3.B). Finally, we discuss some noises extrinsic to the fiber (Section 4), which by dint of their insidious and ubiquitous character afflict all applications of precision fiber interferometry.

3. INTRINSIC NOISES IN SOLID-CORE OPTICAL FIBER INTERFEROMETRY

A. Linear Noise Sources

1. Rayleigh Scattering

One of the most basic of optical noises in a waveguide is that due to scattering from static surface roughness and density variations. The interference of this randomly Rayleigh-scattered field with the incident field can manifest as optical noise [38–41]. The magnitude of this noise depends on the interplay between the coherence length of the light source and that of the density variations [39], and the efficiency with which the scattered field is mode matched with the incident one. In an optical fiber, only a small fraction of the Rayleigh backscattered light is recaptured [38].

The main concern in a fiber Michelson interferometer is the first order backscattering process, while Mach–Zehnder geometries suffer from double Rayleigh backscattered (DRB) light. For the MZI considered in this paper, the field at the end of each arm is the sum of the incident (forward propagating) field and the DRB field. Assuming that the polarization does not change along the

fiber (this represents the worst case scenario), the DRB field exiting the ith arm is [41]

$$\delta E_i^{\mathrm{DRB}}(t) = \int_0^{L_i} \mathrm{d}z' \int_0^{z'} \mathrm{d}z E_0\left(t - \tau_i - \frac{2(z'-z)n}{c}\right)$$

$$\times e^{-(\frac{\alpha}{2}+i\beta)[L_i+2(z'-z)]}\rho_i(z')\rho_i(z), \quad (2)$$

where $E_0(t) \equiv E_0 \exp(i\delta\psi(t))$ is the field at the entrance of the MZI (with phase fluctuations $\delta\psi$), $L_i = c\tau_i/n$ the arm length (with n the refractive index), and α, β respectively the power attenuation (in units of m^{-1}) and the propagation constant in the fiber. The random field $\rho_i(z)$ describes the fraction of light randomly scattered per unit length at position z along the ith fiber; it is modeled by a circular white Gaussian zero-mean process (assumed to be uncorrelated between the two fiber arms) [39–41]: $\langle\rho_i^*(z)\rho_j(z')\rangle = \alpha_s \mathcal{S}\delta_{ij}\delta(z-z')$, where α_s is the scattering cross section and $\mathcal{S}$ the recapture efficiency. The field that subsequently exits the MZI and illuminates the detectors A, B (see Fig. 2) are

$$E_{A,B}(t) = \frac{1}{2}[E_1(t) + \delta E_1^{\mathrm{DRB}}(t)] \pm \frac{1}{2}[E_2(t) + \delta E_2^{\mathrm{DRB}}(t)], \quad (3)$$

where we have assumed that the entrance and exit couplers are symmetric (the configuration that minimizes noise coupling), and $E_i(t) = E_0(t - \tau_i) \exp[-(\frac{\alpha}{2} + i\beta)L_i]$ is the mean field exiting the ith arm. With balanced detection, i.e., when the outputs of the two detectors are subtracted with equal gain, the resulting fluctuations in the homodyne photocurrent are

$$\delta i_{\text{hom}}(t) \propto 2\text{Re}\left[E_1^*(t)\delta E_2^{\text{DRB}}(t) + E_2^*(t)\delta E_1^{\text{DRB}}(t)\right]. \quad (4)$$

Fluctuations in the photocurrent can be referred to apparent phase noise. In the regime of interest—where the laser coherence time t_c is much longer than the light travel time in the arms—we estimate the DRB phase noise spectrum as (see Supplement 1)

$$S_\phi^{\text{DRB}}(\omega) = \frac{5}{9}\left(\frac{\alpha_s \mathcal{S}}{2\alpha}\right)^2 (2\alpha L_{\max} + e^{-2\alpha L_{\max}} - 1)\frac{2t_c}{1 + (\omega t_c)^2}. \quad (5)$$

Here, $L_{\max}$ is the larger of the two arm lengths, and an extra factor of 5/9 accounts for depolarization due to DRB [42]. Importantly, the DRB-induced phase noise scales as $1/t_c$ in the limit of laser coherence time much longer than the observation time (which, for state-of-the-art CW lasers [11,12], is $\omega \gtrsim 2\pi \cdot 20$ mHz). [Note that DRB in the input fiber lead can be assumed to add to the relative intensity noise (RIN) for narrow-linewidth lasers [43,44].]

2. Thermodynamic Phase Noises

The fact that the optical fiber is in thermal equilibrium at a temperature T produces fundamental thermodynamic fluctuations in its geometric and material properties that appear as apparent phase noise.

Thermoconductive noise [45–49]. The dissipation of heat in the fiber material causes apparent fluctuations in temperature. Since the phase acquired by light passing through a medium of (effective) refractive index n and length L is knL ($k = 2\pi/\lambda$ is the magnitude of the wave vector), temperature fluctuations can manifest as apparent phase fluctuations via the temperature-dependent expansion of the fiber, and via the temperature-dependent changes in the refractive index. The resulting phase noise is [47]

$$S_\phi^{\text{TC}}(\omega) = \frac{4\pi^2 L^2}{\lambda^2}\left(\frac{\mathrm{d}n}{\mathrm{d}T} + n\alpha_L\right)^2 S_{\delta T}(\omega), \quad (6)$$

where, $\alpha_L = (1/L)\,\mathrm{d}L/\mathrm{d}T$ is the temperature coefficient of length expansion.

The apparent temperature noise $S_{\delta T}$ follows from the fluctuation dissipation theorem [50,51] (FDT). The so-called "direct form" of the FDT [52] implies that any dissipated thermal power in the medium W_{diss} results in a temperature fluctuation, $S_{\delta T}(\omega) = (8k_B T/\omega^2)(W_{\text{diss}}/Q_0^2)$, where Q_0 is the magnitude of the heat injected at frequency ω. For a Gaussian optical beam with a mode field radius r_{mf} propagating through a fiber core of thermal conductivity κ, the FDT implies that [48]

$$S_{\delta T}(\omega) = \frac{k_B T^2}{\pi \kappa L}\text{Re}[e^{(i\omega r_{\text{mf}}^2)/(4D)}\text{E}_1(e^{(i\omega r_{\text{mf}}^2)/(4D)})]. \quad (7)$$

Here, $\text{E}_1(x) = \int_x^\infty t^{-1}e^{-t}\mathrm{d}t$ is the exponential integral function, and $D = \kappa/C_V$ is the thermal diffusivity (assuming a volumetric heat capacity at constant volume C_V). The above expression can be approximated by the so-called Wanser formula [46,47]

$$S_{\delta T}(\omega) = \frac{k_B T^2}{2\pi \kappa L}\ln\left[\frac{k_{\max}^4 + \frac{\omega^2}{D^2}}{k_{\min}^4 + \frac{\omega^2}{D^2}}\right], \quad (8)$$

with $k_{\max} = 2/r_{\text{mf}}$ and $k_{\min} \approx 2.405/a$ (a being the fiber outer radius). A comprehensive table of constants can be found in Supplement 1.

Thermomechanical noise. Thermoconductive noises ultimately arise due to thermal dissipation—and associated temperature fluctuations—in the active region of the optical fiber. By contrast, thermomechanical noise is due to mechanical dissipation, causing Brownian motion of the lengthwise elastic continuum that constitutes the fiber medium [53].

The 1D elastic continuum of the fiber length can be described as a sum of normal mode harmonic oscillators, each at a frequency $\omega_\ell = (\ell\pi/L)\sqrt{E/\rho}$ (E is the elastic modulus and ρ the mass density), modal mass $m_\ell = \rho AL/2$ (A the transverse area), and loss angle $\phi_\ell(\omega)$ (which is experimentally determined). The loss angle quantifies the imaginary part of the complex spring constant assumed in the structural damping model [54], and represents the degree of anelasticity. Knowing the admittance of each normal mode in terms of these parameters, the FDT predicts an apparent length fluctuation due to thermomechanical noise [48]:

$$S_L^{\text{TM}}(\omega) = \frac{4k_B T}{\omega}\sum_\ell \frac{\omega_\ell^2 \phi_\ell(\omega)}{m_\ell[(\omega^2 - \omega_\ell^2)^2 + \omega_\ell^4 \phi_\ell^2(\omega)]}. \quad (9)$$

If the loss angle is assumed frequency independent and uniform for all modes, i.e., $\phi_\ell(\omega) = \phi_0$, the above expression reduces, in the low-frequency regime (i.e., $\omega \ll \omega_\ell$), to

$$S_L^{\text{TM}}(\omega) \approx \frac{4k_B T L \phi_0}{3AE}\frac{1}{\omega}. \quad (10)$$

These length fluctuations can be referred to apparent phase noise:

$$S_\phi^{\text{TM}}(\omega) = \left(\frac{2\pi n}{\lambda}\right)^2 S_L^{\text{TM}}(\omega). \quad (11)$$

The frequency scaling suggests that thermomechanical noise dominates thermoconductive noise at low frequencies, and ultimately limits the long-term phase stability of long optical fiber links. The latter conclusion, however, relies on the poorly understood low-frequency behavior of the loss angle $\phi(\omega)$.

The sum of thermomechanical and thermoconductive noise, $S_\phi^{\text{therm}} = S_\phi^{\text{TM}}(\omega) + S_\phi^{\text{TC}}(\omega)$, is in excellent agreement with experimental results for frequencies down to about 0.2 Hz [49,55]. However, even though the overall shape and magnitude of the observed spectrum follows these models, the resonances predicted by the thermomechanical theory have not apparently been observed. Together with the measured deviations at lower frequencies, where it is not clear whether the deviations below 0.2 Hz are of a technical or fundamental nature, this indicates the need for future investigations.

Guided acoustic-wave Brillouin scattering. First observed in the context of squeezing quantum optical fluctuations using optical fibers [56,57], guided acoustic-wave Brillouin scattering (GAWBS) refers to the scattering of light into the propagation direction by *transverse* acoustic modes of the optical fiber. Unlike Brillouin scattering (described in Section 3.B), which is stimulated by light, GAWBS is seeded by thermal fluctuations of the acoustic modes and is therefore independent of the optical power in the fiber.

The dominant acoustic modes of the fiber responsible for GAWBS are the transverse radial "breathing" modes and radial "torsional" modes with a near-zero longitudinal wave vector. The former mediates random scattering in the propagation direction—through the photo-elastic effect—akin to pure phase noise, whereas the latter can additionally produce polarization

noise due to birefringence fluctuations. Consequently, they are labeled depolarized modes, whereas the pure radial components are called polarized modes. As far as phase noise is concerned, the primary contribution for single-mode fibers (SMFs) is due to the polarized modes (more so at low frequencies) [58]. Therefore, here we restrict attention to the polarized modes.

The elastic equations in the cylindrically symmetric frame of the optical fiber dictates the behavior of polarized modes. Assuming free boundary conditions, the various normal mode frequencies are given by $\omega_\ell = (v_L/a)y_\ell$, where v_L is the longitudinal acoustic velocity, a is the fiber radius, and y_ℓ satisfies the characteristic equation $(1 - \alpha^2)J_0(y_\ell) - \alpha^2 J_2(y_\ell) = 0$, with J_ℓ the Bessel function of order ℓ; here, $\alpha = v_T/v_L$, and v_T is the transverse acoustic velocity. Each frequency mode corresponds to the elastic radial motion of the fiber, which can be described by an eigenfunction, $U_\ell(r, t) = C_\ell(t)J_1(y_\ell r/a)$, whose amplitude, C_ℓ, has the rms value $\sqrt{\langle C_\ell^2 \rangle} = \sqrt{k_B T/(m_\ell \omega_\ell^2)}$ due to the equipartition principle [59]. Here, $m_\ell = \pi a^2 L \rho \int_0^1 J_1^2(y_\ell x)x\,dx$ is the effective mass of the mode and L the fiber length.

The photo-elastic effect determines the influence of this radial strain on the propagating optical field. Denoting by P_{ij} the components of the photo-elastic tensor, the refractive index fluctuations are given by [57]

$$\delta n(r, t) = \sum_\ell \frac{n_{\text{eff}}^3(P_{11} + P_{12})C_\ell(t)}{2}$$
$$\times \left(\frac{2}{r}J_1\left(\frac{y_\ell r}{a}\right) - \frac{y_\ell}{a}J_2\left(\frac{y_\ell r}{a}\right) \right). \quad (12)$$

The refractive index seen by the light is the average of this expression over the optical mode profile of the fundamental LP_{01} mode of the fiber core. In a SMF, where most of the optical field is confined to the core, we have that $y_\ell r/a \ll \pi$, implying that the first- and second-order Bessel functions in Eq. (12) can be approximated by $y_\ell r/(2a)$ and $y_\ell^2 r^2/(8a^2)$, respectively; then the refractive index change can be approximated by $\delta n \approx n_{\text{eff}}^3(P_{11} + P_{12})\sum_\ell C_\ell(t)y_\ell/(2a)$. Referring to a phase noise, $\delta\phi_{\text{GAWBS}}^{\text{radial}} = (kL)\delta n = (kL)n_{\text{eff}}^3(P_{11} + P_{12})\sum_\ell C_\ell(t)y_\ell/(2a)$, from which it follows that

$$S_\phi^{\text{GAWBS}}(\omega) = \left(\frac{kLn_{\text{eff}}^3(P_{11} + P_{12})}{2a} \right)^2 \sum_\ell y_\ell^2 S_{C_\ell}(\omega). \quad (13)$$

Treating the elastic normal modes as harmonic oscillators with loss angles $\phi_\ell(\omega)$, the spectrum of their amplitudes, S_{C_ℓ}, has the form of a single term in Eq. (9). Just as in the case of thermomechanical noise, the question of the behavior of the loss angle at low frequencies seems to be poorly understood. For example, if loss is assumed to be due to internal dissipation [54] (and thus ϕ being independent of ω over a large range of frequencies), then the phase noise due to GAWBS would exhibit a $1/\omega$ behavior at low frequencies, whose magnitude seems inconsistent with some low-frequency measurements [49,55]; on the other hand, a "velocity-damped" model for mechanical loss ($\phi \propto \omega$) would predict frequency-independent noise due to GAWBS; however, such a loss model is inconsistent with fused silica [60]. The model correctly predicts the resonance frequencies, and for frequencies

around the first resonance ($\omega_1 = (v_L/a)y_1$) and above, the magnitude of the spectrum is in good agreement with experimental data, for both polarized [61] and depolarized [58,62] GAWBS.

The treatment of radial–torsional modes can be obtained analogously, with a different characteristic equation leading to a more complex spectral distribution. The dependence on the azimuthal angle of these modes produces a fluctuating birefringence in the fiber leading to depolarization [62,63].

3. Polarization Noise

An ideal straight segment of fiber is cylindrically symmetric about its length, implying that the polarization state of light propagating in it is two-fold degenerate, i.e., any orthogonal pair of polarization states propagates through it with the same propagation constant. Real-world non-idealities such as imperfections during the manufacturing process or extrinsic factors such as stresses (from bending or twisting), and environmental perturbations can lift this degeneracy, leading to birefringence. Fluctuations in the birefringence will cause the polarization to fluctuate.

The polarization evolution along a fiber can be conveniently described as the action of a 4×4 Müller matrix on an input polarization state, $\hat{s}_i$, represented as a Stokes vector in a Poincaré ball [64]. Since most modern fiber components show negligible polarization-dependent loss, the Stokes vector is confined to its surface. The transformation of the polarization state can then be visualized as a simple rotation. Each polarization state corresponds to a single point on the sphere's surface, where all linear polarization states lie on the equator and left- and right-circular states are located at the two poles. Within this picture, it is easy to see that whenever the input polarization is aligned with one of the two eigenvectors of the Müller matrix of the fiber, polarization is preserved during transmission [65]. There exist alternate conventions for choice of polarization bases in the literature. For example, for narrow-linewidth light sources, one could choose polarization bases that are orthogonal with respect to the output of the fiber [66]. Or, polarization bases can be chosen so as to be invariant to the polarization mode dispersion of the fiber [67], which have the advantage of being insensitive to frequency changes in the fiber to first order [68].

In an interferometer, where each path is in general independent, the same input state is transformed to a different output state. Since the interference depends on their overlap, random birefringence fluctuations in the two arms or the input fiber cause variations in the visibility factor, the low-frequency part of this effect being called polarization-induced fading (PIF) [65,69] (see Supplement 1 for more details). Additionally, these fluctuations can induce apparent output phase noise that can be minimized by maximizing the visibility [65,70,71]. Several techniques have been documented to evade PIF: (a) use of polarization-maintaining (PM) fibers, although PM fibers are unsuitable for precision interferometry due to their higher loss and dependence on operating conditions [72]; (b) polarization diversity reception [72], where three independently polarized receivers are used to ensure that perfect interference (at DC) happens in at least one of them—the trade-off is a significant reduction of contrast due to losses; (c) active control of the birefringence of the output fiber lead [73], or input polarization [74]; (d) use of Faraday mirrors (in a Michelson topology) [75]. Some combination of these techniques may enable recovery of visibility.

A far more insidious effect is thermodynamic fluctuations of the birefringence of a non-ideal fiber (or a PM fiber) [76], which can manifest as broadband phase *and* amplitude noise. For an amorphous material such as fused silica that forms the core of a SMF, this variety of thermodynamic polarization noise is sub-dominant to the other thermodynamic phase noises.

B. Nonlinear Noise Mechanisms

Nonlinear optical activity of fused silica—the major component of the core of single-mode optical fiber—can lead to optical noises stimulated by the field propagating through it. Because the silica molecule possesses inversion symmetry, all even-order electric susceptibilities vanish. Thus, the leading order optical nonlinearity is mediated by the third-order electric susceptibility $\chi^{(3)}$. As we shall now see, it suffices to describe a majority of relevant nonlinear noise effects found in optical fibers [77].

Kerr effect. The optical intensity of light propagating down a fiber can change its refractive index:

$$n(I) = n_0 + \frac{3 \, \mathrm{Re}\{\chi^{(3)}\}}{4\epsilon_0 c \, n_0^2} I \equiv n_0 + n_2 I; \quad (14)$$

here, $n_0 = \sqrt{1 + \mathrm{Re}\{\chi^{(1)}\}^2}$ is the (effective) linear refractive index, and $I = P_0/A_{\mathrm{eff}}$ is the optical intensity due to the (average) power P_0 focused in a transverse area, $A_{\mathrm{eff}} \approx \pi r_{\mathrm{mf}}^2$.

If light of a single frequency is propagating down the fiber, the intensity-dependent refractive index leads to self-phase modulation (SPM). This is captured by the additional phase, $\phi_{\mathrm{SPM}} = k n_2 L_{\mathrm{eff}} I$, accumulated over an effective fiber length, $L_{\mathrm{eff}} = (1 - \exp[-\alpha l])/\alpha$, where the linear absorption coefficient α is measured in m^{-1}. (The effective length is the length of a lossless fiber having the same nonlinear impact as a lossy fiber with exponentially decaying intensity along its length. For modern commercially available fibers with attenuation coefficients as low as $\alpha \approx 0.16$ dB km^{-1}, the effective length is $L_{\mathrm{eff}} \lesssim 27$ km.) The SPM mechanism can transduce laser power fluctuations, δP, into phase fluctuations:

$$\delta\phi_{\mathrm{SPM}} = \gamma L_{\mathrm{eff}} \delta P, \quad (15)$$

where we combined the fiber properties for a given wavelength in the nonlinear coefficient $\gamma = k n_2/A_{\mathrm{eff}}$.

In an interferometer, the coupling between intensity fluctuations of the light source and output phase noise crucially depends on the splitting ratio of the first FC and the two arm lengths of the interferometer. For an interferometer with a perfect 50/50 splitting ratio of the first FC, one obtains (see Supplement 1)

$$S_\phi^{\mathrm{SPM}}(\omega) = \left(\frac{4\gamma P_0}{9}\right)^2 |L_{\mathrm{eff},1} - e^{-i\omega\tau} L_{\mathrm{eff},2}|^2 S_{\mathrm{RIN}}(\omega), \quad (16)$$

where τ denotes the time delay between the arms, $L_{\mathrm{eff},i}$ is the effective length of the ith arm, and S_{RIN} is the relative intensity noise (RIN) spectrum. An extra factor of 8/9 was introduced to account for the random polarization evolution in a standard fiber [78,79] (this factor is absent for PM fiber arms). If the two arms of the interferometer are equal in length, i.e., $\tau = 0$ and $L_{\mathrm{eff},1} = L_{\mathrm{eff},2}$, the fluctuations at the output are correlated and the noise due to SPM vanishes. For a finite but small length difference, $L_{\mathrm{eff},1} \approx L_{\mathrm{eff},2} = L_{\mathrm{eff}}$, the square of the absolute value in Eq. (16)

reduces to $4L_{\mathrm{eff}}^2 \sin^2(\omega\tau/2)$. Finally, when one arm is substantially longer, e.g., $L_2 \ll L_1 \approx L_{\mathrm{eff}}$, the same term reduces to L_{eff}^2.

If light of multiple frequencies is present in the fiber, the intensity of one field can modulate the phase of another, an effect called cross-phase modulation (XPM) [77]. XPM is effective only for those fields whose spatial overlap is significant, which explains its significance in the core of an optical fiber. For a pair of fields (labeled with indices i, j) of identical polarization, it can be shown that the refractive index experienced by the ith field is modulated by the jth field's intensity I_j according to [77]

$$n_i(I_j) = n_{0,i} + n_{2,i} I_i + 2n_{2,i} I_j, \quad (17)$$

capturing both SPM and XPM. This implies that the phase of the ith field is modulated as

$$\delta\phi_{\mathrm{XPM}}^i = 2\gamma_i L_{\mathrm{eff}} \delta P_j, \quad (18)$$

where $\gamma_i = k n_{2,i}/A_{\mathrm{eff}}$. In an interferometer, where the first FC has 50% transmission, the induced phase noise in the ith beam is related to the intensity noise of the jth beam via

$$S_{\phi,i}^{\mathrm{XPM}}(\omega) = \left(\frac{8\gamma P_{0j}}{9}\right)^2 |L_{\mathrm{eff},1} - e^{-i\omega\tau} L_{\mathrm{eff},2}|^2 S_{\mathrm{RIN}}^j(\omega), \quad (19)$$

where again complete polarization scrambling is accounted for by a factor of 8/9. Such models, particularly for XPM, were developed in comparatively recent perturbative approaches [80–83] that detail the Kerr effect not only in its single- and multi-channel forms, but also for stochastic variants (arising with amplified spontaneous emission, for example) and for arbitrary pulse shape. Indeed, in characterizing a large fraction of SPM and XPM as phase noise, the models pave the way for noise cancellation using long-temporal correlations [81].

Generalizing further, any third-order nonlinear interaction among three waves producing a fourth in the process is called four-wave mixing (FWM). This mixing is of particular importance for wavelength division multiplexing, where the frequencies are equally spaced and significant cross talk between channels can occur [84]. FWM does not contribute noise in optical interferometry, but rather produces nonlinear power losses depending on the phases of the involved fields. If only two input fields are present (at frequencies $\omega_{1,2}$), secondary waves at frequencies $\omega_3 = 2\omega_1 - \omega_2 = \omega_1 - \Delta\omega$ and $\omega_4 = 2\omega_2 - \omega_1 = \omega_2 + \Delta\omega$, with $\Delta\omega = \omega_2 - \omega_1$, are created. These frequencies are of particular interest because they appear close to the ones of the two input fields, ω_1 and ω_2, provided that $|\Delta\omega| \ll \omega_{1,2}$. The power transfer from the primary to the secondary waves can be expressed as [85–87]

$$P_3 = \eta (\gamma L_{\mathrm{eff}})^2 P_1^2 P_2 e^{-\alpha L}, \quad (20)$$

with the scattering efficiency,

$$\eta = \frac{\alpha^2}{\alpha^2 + \Delta\beta^2} \left(1 + \frac{4e^{-\alpha L} \sin^2(\Delta\beta L/2)}{(1 - e^{-\alpha L})^2}\right), \quad (21)$$

depending strongly on the phase matching between primary and secondary waves. The power scattered into the fourth beam, P_4, is obtained by interchanging P_1 and P_2 in Eq. (20).

The phase mismatches for ω_3 and ω_4 can be written as $\Delta\beta_3 = 2\beta(\omega_1) - \beta(\omega_2) - \beta(\omega_3)$ and $\Delta\beta_4 = 2\beta(\omega_2) - \beta(\omega_1) - \beta(\omega_4)$, respectively. Taylor expanding the propagation constants

up to third order in ω around the central frequency, $\omega_0 = (\omega_1 + \omega_2)/2$, results in [86,88]

$$\Delta\beta_{3,4} = -\frac{d^2\beta}{d\omega^2}|_{\omega_0}\Delta\omega^2 \pm \frac{1}{2}\frac{d^3\beta}{d\omega^3}|_{\omega_0}\Delta\omega^3$$

$$= \frac{2\pi c\,\Delta\lambda^2}{\lambda_0^2}\left(D(\lambda_0) \pm \frac{\Delta\lambda}{2}\frac{dD}{d\lambda}|_{\lambda_0}\right), \qquad (22)$$

with the plus sign for $\Delta\beta_3$ and the minus sign for $\Delta\beta_4$. To obtain the wavelength-dependent expression, the dispersion parameters $D(\lambda) = d/d\lambda(d\beta/d\omega) = (-2\pi c/\lambda^2)d^2\beta/d\omega^2$ and $\Delta\lambda = \lambda_1 - \lambda_2$ were used. The phase mismatch should be as large as possible to avoid efficient FWM and thus high nonlinear losses in the primary waves.

Stimulated Brillouin and Raman scattering. Inelastic scattering of optical photons by acoustic or optical phonons, which represent the mechanical vibrations of the fiber medium, is another important class of nonlinear effects in optical fibers. This manifests as optical loss into the mechanical modes. When the mechanical mode is at acoustic frequencies, the effect is called Brillouin scattering, while if the phonons are at optical frequencies, it is termed Raman scattering. Their effect is two-fold: they primarily limit the optical power that can be employed but can also transduce noise from the phonon field onto the optical field. The consequence of an optical power threshold is that by limiting the usable power, the attainable signal-to-shot-noise ratio (at large Fourier frequencies, where shot noise can dominate extraneous noises), which scales as $1/\sqrt{P}$, is limited.

The optical threshold due to stimulated Brillouin scattering (SBS) arises as follows. The pump field beats with the spontaneously backscattered acoustic Stokes waves [89]. The resulting interference pattern changes the material density via electrostriction, creating a forward propagating refractive index grating from which more pump photons are backscattered. As soon as a certain threshold pump power is reached, the Stokes wave builds up rapidly and limits the transmittable power. A good approximation to estimate the Brillouin threshold in standard single-mode step-index fibers is [90]

$$P_{th,B} = \frac{\kappa K A_{eff}}{g_B L_{eff}}, \qquad (23)$$

where g_B is the Brillouin gain coefficient, which is the value of the Lorentzian-shaped Brillouin gain spectrum at the Brillouin frequency ω_B. For standard single-mode silica fibers, $\omega_B \approx 2\pi \cdot 11$ GHz [91], with $g_B \approx 1.68 \times 10^{-11}$ mW^{-1} at 1550 nm. The numerical factor $\kappa \approx 19$ accounts for modern low-loss optical fibers [92]. The mixing efficiency K between the pump and the Stokes wave depends on the input polarization as well as the properties of the fiber. For a completely scrambled input polarization, $K \approx 3/2$, while for fibers with negligible birefringence and linear input polarization, $K = 1$ [93]. Note that this simple formula does not account for other fiber geometries, and the effective area needs to be replaced by the acousto-optic effective area [94,95].

Stimulated Raman scattering (SRS), on the other hand, involves photon scattering off of molecular vibrations of the constituents of the fiber, which oscillate at $\omega_R \gtrsim 2\pi \cdot 10$ THz. In this process, forward and backward scattering of both Stokes and anti-Stokes light is possible, where the latter is nevertheless typically much weaker due to the limited number of excited optical

phonons at thermal equilibrium ($k_B T/\hbar\omega_R \ll 1$). In the absence of a second input field, with a frequency difference close to the molecular resonance frequency, the stimulated process builds up from noise. The interference between the two fields then drives the molecular resonances, creating a positive feedback loop leading to the stimulated process. Under the assumption of a Lorentzian gain profile, the threshold power, defined as input pump power for which Stokes and pump powers are equal at the fiber output, for forward SRS is given by [90]

$$P_{th,R} = \frac{16\,p\,A_{eff}}{g_R L_{eff}}, \qquad (24)$$

where p ranges from one for overlapping and two for completely scrambled polarization between the pump and the Stokes wave. The numerical factor of 16 needs to be replaced by 20 for backward scattering, which is why it is rarely observed in fibers due to the almost exponential increase of Stokes power beyond the threshold. The Raman gain coefficient, g_R, denotes the maximal value of the Raman gain spectrum. For standard SMFs, the peak occurs at a frequency difference between the pump and Stokes wave of about 13.2 THz, where $g_R \approx 1.1 \times 10^{-13}$ mW^{-1} at 1550 nm [96]. Even though the gain coefficient is about two orders of magnitude lower than the one for SBS, the short lifetimes of optical phonons make the gain spectrum for the Raman interaction about six orders of magnitude wider ($\sim$40 THz). This is a very attractive feature exploited in Raman amplifiers, where signal frequencies can be amplified over a broad range as long as the pump wave is chosen such that their frequency difference falls within the spectrum.

From the two nonlinear scattering processes described above, SBS is in optical fiber interferometry by far more critical due to the larger gain coefficient, $P_{th,B}/P_{th,R} \approx g_R/g_B \approx 10^{-2}$. Beyond the threshold power, the backreflected Stokes wave experiences a very rapid growth while at the same time depleting the pump. Once a maximal level is reached, any additional incident power is reflected towards the front end of the fiber, limiting the usable power at the other end. Even though SBS does not directly contribute to phase noise, it affects other power sensitive noise terms such as shot noise. For long, high-performance optical fibers with $L_{eff} \approx \alpha^{-1} \approx 27$ km, the Brillouin threshold for a pump wavelength at 1550 nm, $K = 3/2$, and $\kappa = 19$ predicted by Eq. (23) is about 5 mW. Assuming the first beam splitter of the interferometer to have 50% transmission, the maximal laser power for long-baseline optical fiber interferometry is about 10 mW.

The noise transduced by both effects is sub-dominant to other linear sources of thermodynamic noise. For Raman scattering, this is due to the fact that Raman-active phonons are not thermally populated at room temperature. For Brillouin-active phonons, their much larger frequencies, compared to the mechanical modes that participate in GAWBS, etc., imply that their contribution is sub-dominant.

4. EXTRINSIC NOISES IN OPTICAL FIBER INTERFEROMETRY

A. Source and Electronic Noise

A real-world laser is a non-ideal oscillator whose output exhibits fluctuations in both its amplitude and phase. Noise in the amplitude is typically characterized through the fluctuations it causes in the optical power, normalized by the average output power of the light source, and is termed RIN. Such power fluctuations are

converted into phase fluctuations and limit the sensitivity of optical interferometers; they are also known to limit the performance of optical communication systems [97]. In an interferometer, the transduction of RIN to output noise depends on the demodulation approach and arm length difference. Assuming the time delay difference between the arms to be much smaller than the correlation time of the power fluctuations, the RIN-equivalent phase noise for active homodyne detection at a single detector is given by S_{RIN}/V^2, which is at best as low as S_{RIN} (when the visibility is $V = 1$), and much worse in general. Balanced detection offers immediate mitigation of this stringent limit by subtraction of the large DC component (see Supplement 1 for details). Assuming 50/50 FCs ($V_A = V_B \equiv V$) and independent photodiodes with adjustable gains, G_A and G_B, the RIN equivalent phase noise is given by

$$S_\phi^{RIN}(\omega) = \left(\frac{\epsilon}{2 G_A R_A V}\right)^2 S_{RIN}(\omega), \qquad (25)$$

where $\epsilon \equiv G_A R_A - G_B R_B$. The RIN contribution is due to both classical and quantum noises, viz., $S_{RIN}(\omega) = S_{RIN}^{classical}(\omega) + 2hc/(\lambda P)$, with h being Planck's constant, c the speed of light, λ the optical wavelength, and P the optical power. Thus, the RIN-equivalent phase noise, proportional to the imbalance ϵ^2, can be made arbitrarily small. (Note, however, that phase noise due to quantum fluctuations, $S_\phi^{quantum} = 2hc/(\lambda P)$, which has the exact same form as RIN from amplitude quantum noise, cannot be suppressed in this fashion.) This conclusion is crucially reliant on precisely maintaining the quadrature demodulation of the homodyne, as small deviations from this point will transduce RIN to apparent phase noise according to $S_\phi^{RIN}(\omega) = \tan^2(\Delta\phi) S_{RIN}(\omega)$, where $\Delta\phi$ is the phase deviation from quadrature, which is typically the dominant transduction process. RIN coupling can also be reduced by choosing a heterodyne detection scheme, where, e.g., with phase-sensitive detection [98], the DC part is suppressed by the low-pass filter during the demodulation process, however, at the expense of a 3 dB reduction in sensitivity.

Laser phase noise refers to phase fluctuations $\delta\psi(t)$ of the electric field, $E(t) = E_0 \exp[i(\omega_0 t + \delta\psi(t))]$. Assuming stationarity, it can be shown that the electric field autocorrelation, $R_E(\tau) \equiv \langle E^*(t) E(t + \tau)\rangle$, is [99,100]

$$R_E(\tau) = E_0^2 \exp\left[i\omega_0\tau - \int_{-\infty}^{\infty} S_{\delta\psi}(\omega) \sin^2\left(\frac{\omega\tau}{2}\right) \frac{d\omega}{2\pi}\right]. \quad (26)$$

It is typical to speak of "frequency noise" as frequency-equivalent phase noise, defined by $\delta\nu \equiv \dot{\delta\psi}/(2\pi)$, for which $S_{\delta\nu}(\omega) = \left(\frac{\omega}{2\pi}\right)^2 S_{\delta\psi}(\omega)$. A less informative, but common, measure of phase noise is the "linewidth," defined as the full-width at half maximum (FWHM) of the electric field power spectral density $S_E(\omega) = \int_{-\infty}^{\infty} R_E(\tau)\exp(-i\omega\tau)d\tau$.

Phase noise in the laser at the input of an interferometer can manifest as an apparent phase signal if there is an optical time delay τ between the two arms when they recombine. At recombination, the phase difference between the two fields due to laser phase noise is $\phi(t) = \delta\psi(t) - \delta\psi(t - \tau)$. Taking the Fourier transform gives the transfer function $(1 - \exp(-i\omega\tau))$ from $\delta\psi$ to ϕ; consequently [101–103],

$$S_\phi(\omega) = 4 \sin^2\left(\frac{\omega\tau}{2}\right) S_{\delta\psi}(\omega)$$

$$= (2\pi\tau)^2 \mathrm{sinc}^2\left(\frac{\omega\tau}{2}\right) S_{\delta\nu}(\omega),$$

where $\mathrm{sinc}(x) = \sin(x)/(x)$. Thus, laser phase or frequency noise directly manifests as an apparent phase signal ϕ sensed by the interferometer. At low Fourier frequencies, i.e., $\omega \ll \tau^{-1}$, $\mathrm{sinc}(\omega\tau/2) \approx 1$, so that $S_\phi(\omega \ll \tau^{-1}) \approx (2\pi\tau)^2 S_{\delta\nu}(\omega)$. The same relation holds for a heterodyne scheme, where the output oscillates at the modulation frequency before it is mixed down to DC in phase-coherent detection.

The final stage of the measurement—the conversion of photons to an electrical signal at the photodetector—can also add noise that is indistinguishable in a single measurement from any phase signal in the interferometer. This type of "dark noise," known as noise-equivalent power (NEP) ($\sim 10^{-12}$ W · Hz$^{-1/2}$ at frequencies $\gtrsim 1$ kHz for modern low-noise photodetectors), originates from noise processes in the photodiode or thermal Johnson noise from the subsequent electronics. However, its effect can be evaded in most cases by employing a succeeding low-noise large-gain (i.e., low-noise-figure) amplifier, or mitigated by subtracting its estimate from an independent reference measurement. A prominent example where detector dark noise cannot be as easily evaded is when the interferometer is fed with non-classical light.

B. Geophysical and Environmental Sources of Noise

Seismic ground motion is relevant at frequencies below 100 Hz. Its origins can range from the mundane—such as anthropogenic and earthquakes—to deeply fundamental aspects of the coupled dynamics of the Earth's core, oceans, and atmosphere [104–106]. The 10−100 Hz region is typically dominated by anthropogenic sources [107], which exhibit significant diurnal and spatial variation, and is thus difficult to model. However, because these disturbances are carried by surface waves, their propagation is attenuated over length scales of a few km. Earthquakes and their aftershocks dominate the ground motion at a few Hz. Below 1 Hz is a sequence of fundamental and universal spectra of seismic and atmospheric noises. The largest of these fundamental sources is the secondary microseism [105,108,109] at 0.1−1 Hz causing vertical ground motion of ~10 μm · Hz$^{-1/2}$; a factor of five smaller is the primary microseism at ~0.02−0.1 Hz; another order of magnitude smaller is the seismic hum [110] at ~1−20 mHz. Correlated with the microseism ground motion are microbarom atmospheric pressure fluctuations of ~(0.1−1) Pa · Hz$^{-1/2}$ at infrasonic frequencies [111,112].

Ground motion causes strain on an optical fiber, which is transduced to apparent phase noise via the strain-optic effect. Assuming a fiber under isotropic stress, the phase change per unit fiber length and pressure (p) is approximately [113] $\delta\phi/(L\delta p) \approx \frac{\beta(1-2\nu)}{2E}(n^2(2P_{12} + P_{11}) - 2)$, where E and ν denote Young's modulus and the Poisson ratio of the fiber, respectively, and n the core refractive index. For modern fibers, $\delta\phi/(L\delta p) \approx 3 \cdot 10^{-5}$ rad Pa^{-1}m^{-1} at $\lambda = 1.55$ μm. If the fiber arms are spooled freely—as a means to fold a long optical path length into a compact space—and placed vertically, the spooled fiber experiences strain [114], $\delta L/L = (\nu_S \rho_S h/4E_S)\delta a$, where ρ_S is the density of the fiber spool, h its height, E_S the Young's modulus, ν_S its Poisson ratio, and δa the local vertical acceleration. The resulting phase noise is

$$S_\phi^{\text{seis}}(\omega) = 2\left(C_{\text{cmrr}} \frac{knLv_S\rho_S h}{4E_S}\right)^2 S_a(\omega), \qquad (27)$$

where C_{cmrr} denotes the common mode rejection ratio (CMRR) accounting for the fraction of seismic noise coupling that is the same along both arms. (In principle, the CMRR can be modeled if the geometry of the arms and correlation length of the seismic field are known; in practice, it is usually measured.) If the fiber is spooled on an elastic core of a length of several meters, atmospheric pressure fluctuations—correlated across similar length scales—can couple into the interferometer [115].

If the fiber interferometer is confined to a region of space smaller than the correlation length of some of these geophysical seismic noises, active vibration isolation can mitigate their effects [55]. For applications where the majority of the optical fiber is outside of the laboratory, temperature changes along the fiber are typically among the most dominant sources of noise. Since both the effective refractive index and the fiber length are functions of temperature, the phase change per unit length and temperature change is [113] $\delta\phi/(L\delta T) \approx k[(n/L)\mathrm{d}L/\mathrm{d}T + \mathrm{d}n/\mathrm{d}T]$. Depending on the fiber used, even hundreds of radians per meter per degree are possible. In general, the combined phase noises of fibers exposed to urban environments over short time scales are Gaussian distributed [116].

Terrestrial gravity fluctuations [117] arise from the geophysical motion of large masses—seismic density waves [118], atmospheric pressure waves, or even the motion of clouds [119]—that couple to the interferometer via direct Newtonian gravity. For example, the typical displacement noise on a $\sim$100 km long spool of optical fiber due to Newtonian noise from the ambient seismic Rayleigh wave field is $\sim 10^{-19}\,\mathrm{m}\cdot\mathrm{Hz}^{-1/2}$ at 10 Hz and falls off roughly as the fourth power of frequency—orders of magnitude smaller than the motion from direct seismic motion. However, terrestrial gravity fluctuations cannot be shielded and thus represent the ultimate achievable limit of sensitivity on Earth.

5. INTRINSIC NOISES IN STRUCTURED-CORE FIBERS

Due to technological advances and theoretical knowledge gained in the last few decades, silica-based optical fibers predicated on total internal reflection (TIR) have reached a point where they can be only marginally improved. The most important parameters for changing the properties in these structures are the choice of material and the concentration of added dopants. To overcome these limitations, optical fibers with alternative light guiding principles have been intensively researched over the last 30 years.

Photonic crystal fibers (PCFs) are optical waveguides with microstructured, periodic transverse refractive index profiles [120]. These microstructured fibers confine light to the core by modified TIR (M-TIR) [121], photonic bandgaps (PBGs) [122–124], or antiresonant (AR) reflection [125]. Waveguides based on M-TIR, termed index guiding fibers, have a solid core surrounded by a periodic air-hole cladding with a lower average refractive index. By changing the size and separation between the holes, they allow for much greater design flexibility as compared to TIR-based fibers [126–128]. In hollow-core fibers (HCFs), light is guided via either PBGs (HC-PBGFs) [129–131] or the anti-resonance occurring at the glass membranes making up the boundary of the fiber core (HC-ARFs) [132,133]. Since light propagates mainly in air in these structures, low-loss guidance with reduced latency, higher

damage thresholds, and weaker nonlinear and thermal impacts are possible.

The properties of PCFs strongly depend on the transverse structure in addition to the choice of materials. Thus, they offer much more flexibility in their design and can be optimized for a wide range of different applications. While the losses in HC-PCBFs remain hampered by high propagation losses (with a lowest documented loss of 1.7 dB/km [24]), HC-ARFs benefit from a smaller overlap of the guided mode with the glass, at 10^{-5} as compared to 10^{-4} in HC-PCBFs [131]. Compounded with advantages in polarization and mode purity, HC-ARFs in particular present a noteworthy alternative to conventional silica-based SMFs for optical fiber interferometry, though we extend the discussion below to both HCF types with the hope of representing a better overview of the available literature.

Rayleigh scattering and attenuation. Due to the low overlap between the optical mode and the silica membranes of properly designed hollow cores, one can naively assume at least 50 dB reduction in the backscattering coefficient. However, it is important to note that scattering in such fibers does not operate through Rayleigh scattering, but rather by scattering related to variations in the core dimensions and surface roughness caused by frozen-in thermally excited surface capillary waves during the fiber draw. Consequently, the actual scattering coefficient in those structures is higher than for conventional SMFs [25,134–136]. Since Rayleigh scattering is one of the main causes of loss at telecom-wavelengths for silica-based fibers, HCFs with low attenuation coefficients are expected to show lower backscattering (controlling for factors such as directivity and recapture coefficient). Negative curvature fibers [133] and in particular doubly nested AR nodeless fibers (DNANFs) [137] have nowadays attenuation coefficients as low as 0.174 dB/km [17] (S/C-band), and are expected to go below 0.1 dB/km in the not too far future. This type of fiber achieved a backscattering coefficient of -118 dB/m, which is more than 40 dB below the one for conventional solid-core fibers [135] and is particularly useful to enhance the sensitivity of fiber optic gyroscopes [138]. Backscattering from the air of an air-filled NANF has also recently been investigated [139].

Thermal noise. Because the thermo-optic coefficient of air is much smaller than the one for fused silica at a constant volume, HCFs show a greatly reduced phase response to external temperature variations [139]. Indeed, the thermal sensitivity of HC-PBGF has been measured to be more than one order of magnitude lower than that of solid-core fibers [140–142]. This is particularly important for applications where the fiber cannot be shielded from the environment, and the interferometric arms do not share common temperature drifts, e.g., for frequency dissemination. By cooling silica-based HCFs, it is even possible to build interferometers that are insensitive to external temperature drifts if operated close to the zero-crossing temperature of the thermal expansion coefficient of fused silica [143,144]. In conventional solid-core fibers, this is possible only at much lower temperatures [145], as they are dominated by the thermo-optic effect and the core and cladding regions have different doping concentrations with different thermal expansion coefficients. The thermal sensitivity can also be lowered by reducing the thickness of the coating and thus its contribution to the thermal expansion, which has been shown to provide an almost 30-fold reduction of thermal sensitivity in NANFs over solid-core fibers [146]. Similarly, PM PCFs show a larger birefringence and a more than 30-fold reduction in the temperature dependence

of birefringence compared with PM solid-core fibers [147]. In addition, the intrinsic thermodynamic fluctuations limiting the performance of conventional fiber interferometers are expected to be much smaller in HCFs, particularly with evacuation. Even absent evacuation, air-filled fibers and have been shown to compare favorably, and even surpass conventional SMF interferometers for some frequency ranges, although the comparison was made for SMFs with very small fiber cores [148]. A recent theoretical and experimental study has painted a clearer picture [149], showing that fundamental noise can indeed be lower in HCFs provided that the core is evacuated and sealed below atmospheric pressure (about 0.15 atm. in [149]).

GAWBS. GAWBS has been intensively studied in both solid-core PCFs [150–155] as well as HCFs [156–159]. The GAWBS spectrum for polarized and depolarized modes can be tailored by adjusting the transverse geometry of the fiber and thus the overlap between the optical and acoustic modes to either weaken its impact or enhance it for sensing applications. In HCFs, the spectrum contains contributions from the optomechanical coupling between the acoustic modes supported by the silica capillaries (cladding) and air (core) with the optical modes [159]. Thus, the type of gas and its pressure are two additional degrees of freedom for tuning the optomechanical coupling. If low phase noise is required, evacuation of the core as for intrinsic thermal noise reduction could be a viable solution.

Polarization. Similar to conventional solid-core fibers, properly designed HC-PBGFs support two nearly degenerate, orthogonal fundamental modes [160]. Even though most of the optical power propagates through air, deformations in the transverse structure induced either during manufacturing or operation can lead to significant polarization mode splitting [161]. Intentional asymmetries in the structure surrounding the core can be used to produce PM HC-PBGFs [25] with extinction ratios of more than 30 dB over hundreds of meters of fiber [162]. With AR fibers, early results indicate the possibility of achieving extremely low polarization mode coupling without intentional birefringence, outperforming conventional and PM fibers by up to three orders of magnitude [163]. Additionally, this level of polarization purity is very robust against environmental perturbations, making AR fibers ideal candidates for high-precision fiber optic sensing.

Nonlinear noise. The ability to change the transverse geometry of PCFs allows to engineer the size of the mode field and thus the intensity inside the fiber, which in turn governs the nonlinear behavior [164]. HCFs also allow the strength of the nonlinearity to be modified by the filling material; when filled with air, the nonlinear interactions and associated phase perturbations are much smaller than those with an appropriate gas or liquid filling [165]. In particular, air-filled HC-PCFs have an effective nonlinearity that is three orders of magnitude lower compared to SMFs [166,167]. This allows to increase the threshold powers for SBS and SRS, which in turn enables higher signal powers to be delivered to the detectors.

6. CONCLUSION

Solid-core optical fibers have come a long way since their introduction as transmission channels for communication systems in the 1970s. Due to continuous technical improvements, optical loss of contemporary solid-core SMFs is only 0.14 dB/km, which makes them very attractive for diverse applications. One particularly useful type is optical fiber interferometry, in which the fibers serve

as both a transmission channel and a transducer for various external perturbations that change the properties of the propagating optical field. Depending on the application, the transduction of these external parameters may manifest as signal or noise, and sensitivity to them may be desirable or extraneous. We have chosen to view the optical fiber as a conduit for phase-sensitive dissemination of light. This view encompasses applications ranging from distribution of a precise frequency reference for optical clock networks to phase reference for quantum optical networks and phase sensing for gravitational-wave detection. These applications are the most technically demanding deployments of optical phase stability and sensing in the current era.

Under laboratory conditions (i.e., thermally and acoustically shielded), the sensitivity of an optical fiber interferometer at low frequencies is limited mainly by fundamental thermodynamic fluctuations and seismic noise. We illustrate the current typically achievable phase noise performance of an optical fiber MZI under ideal laboratory conditions in Fig. 3. With a fiber attenuation coefficient of 0.16 dB/km (best commercially available fiber), the maximal power per arm is restricted to 12 mW right under the SBS threshold. That power also allows us to ignore nonlinear losses from SRS. As the noise budget suggests, seismic and fundamental thermal phase noises dominate at frequencies below about 100 kHz. Note, however, that according to current theory, GAWBS appears to be the dominant source of noise, which, however, does not reflect the results obtained in thermal noise measurements, indicating a discrepancy in the understanding of acoustic losses that dictate GAWBS at low frequencies. Careful investigation of the broadband acoustic loss of the GAWBS mode is necessary to resolve this inconsistency. A similar inconsistency exists for thermomechanical noise, whose predicted resonance peaks—originating in the normal mode expansion (each mode is treated as a harmonic oscillator)—were not observed [49,55]. In this plot, DRB is negligible due to the small recapture and Rayleigh scattering coefficients. Assuming a short input fiber lead, the conversion between laser frequency to intensity noise due to DRB at the input can also be safely ignored. The RIN coupling is shown for a typical commercially available narrow-bandwidth fiber laser and assuming a balanced homodyne demodulation scheme, where the gains of the photodiodes are equal to within ∼10 ppm. Shot noise is calculated for the interferometer operating at quadrature with 50/50 FCs and equal visibilities of 0.9 at both detectors with a quantum efficiency of 0.9 each. For the arm length imbalance of $\Delta L = 1$ m assumed here, the transduction of the frequency noise of a commercial fiber laser onto output phase noise is still sub-dominant to fundamental thermal noises. For more significant length differences between the arms, e.g., in the largely imbalanced interferometers used for the dissemination of optical frequencies, frequency noise is subdominant to environmental noises [170] but would exceed the thermal noise floor in carefully designed laboratory experiments. Finally, at the relatively low input powers we assume here, together with the monochromaticity of the input light, and nearly equal arms lengths, the effects of SPM, XPM, and FWM are also negligible.

One of the most demanding applications for such an interferometer (in a Michelson configuration) is gravitational wave detection. (In fact, the optical fiber technology available in the 1980s was examined in this context [171].) Although a fiber-based interferometer would reduce the operational costs and provide other advantages—such as single-spatial-mode propagation, much
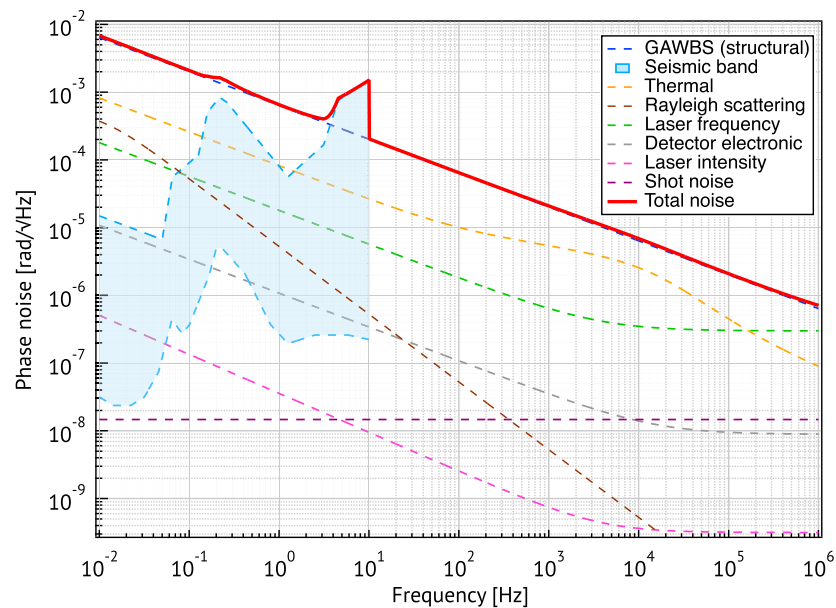
Fig. 3. Projected low-frequency sensitivity of a 10 km fiber interferometer, pumped with 12 mW power (see text for details), with an arm length imbalance of 1 m. Sensitivity is primarily limited by a combination of thermodynamic, and seismic noises at frequencies up to a MHz, with some contribution from DRB around mHz frequencies. The primary thermodynamic contribution is from GAWBS, here assumed to exhibit the typical structural damping mechanism. Other thermodynamic noises, originating from thermal dissipation, lurk less than an order of magnitude below. Seismic noise is estimated using known models for the PSD distribution of global ambient seismic surveys [107,168,169]. (Other relevant parameters used to produce this plot are available in Supplement 1.)

reduced vacuum requirements, and compact geometries—the obtainable phase sensitivity is still orders of magnitude worse than contemporaneous free-space multi-km interferometers (which realize 10^{-9} rad/$\sqrt{\text{Hz}}$ at 100 Hz). Even in the absence of thermal noise, SBS would limit the amount of usable power and thus establish an unacceptably high level of shot noise. Optical fiber interferometers can also potentially be used for other fundamental applications, such as testing the interplay between general relativity and quantum physics with light [172–178]. Again, fundamental thermal noise sets the sensitivity limit, which is, nevertheless, much less demanding compared to gravitational wave detection.

Long optical fibers are most frequently used outside the laboratory, for sending light signals between spatially separated locations. The noise caused by environmental perturbations typically exceeds thermodynamic noise by orders of magnitude, which is why in many practical applications, the fiber is embedded in an interferometer for active phase stabilization. This allows, for example, the dissemination of optical frequency standards over distances up to almost 2000 km [179–183]. A related field is relativistic geodesy, where the clock rates of optical frequency standards are compared via optical fiber links to gain information about differences in gravitational potentials between sites [184,185]. It is truly remarkable that actively stabilized optical fiber interferometers provide enough stability to use general relativistic time dilation as a tool to measure differences in altitude. Interferometric phase stability is also required for many quantum communication protocols [116,186], for example, in the recently much acclaimed field of twin-field quantum key distribution [187,188], which avoids the need for quantum repeaters between the sites.

Taken together, it seems that solid-core optical fiber technology is quite mature, with little room for further improvement in noise performance, except for a lack of complete understanding of thermo-optic losses at infrasonic (<10 Hz) frequencies.

Rapid development in the past few years in the production of structured-core optical fibers with losses approaching those of solid-core fibers offers a potential roadmap for optical-fiber-based platforms for quantum technology and precision measurements. The scanty state of knowledge of the noise processes in these fibers is an open invitation for academic research. Although it is hard to imagine an orders of magnitude improvement in noise properties in such fibers, any improvement will break the barrier of diminishing returns observed in the solid-core fiber platform and will therefore produce new opportunities for science and technology. In particular, HCFs are a promising platform to come close to the sensitivity performance of free-space interferometers, while keeping advantages such as single-spatial-mode operation, ease of deployment, and operational costs.

Data availability. No data were generated or analyzed in the presented research.

Supplemental document. See Supplement 1 for supporting content.

†These authors contributed equally to this work.

REFERENCES

1. K. C. Kao and G. A. Hockham, "Dielectric-fibre surface waveguides for optical frequencies," Proc. Inst. Electr. Eng. **113**, 1151–1158 (1966).

2. J. Hecht, *City of Light: The Story of Fiber Optics* (Oxford University, 1999).

3. R. W. Douglas, "Fifty years of glass technology," Nature **212**, 769–774 (1966).

4. C. Kurkjian, J. Krause, and M. Matthewson, "Strength and fatigue of silica optical fibers," J. Lightwave Technol. **7**, 1360–1370 (1989).

5. J. B. MacChesney and D. J. DiGiovanni, "Materials development of optical fiber," J. Am. Ceram. Soc. **73**, 3537–3556 (1990).

6. P. D. Dragic, M. Cavillon, and J. Ballato, "Materials for optical fiber lasers: A review," Appl. Phys. Rev. **5**, 041301 (2018).

7. R. Olshansky, "Propagation in glass optical waveguides," Rev. Mod. Phys. **51**, 341–367 (1979).

8. Y. Tamura, H. Sakuma, K. Morita, M. Suzuki, Y. Yamamoto, K. Shimada, Y. Honma, K. Sohma, T. Fujii, and T. Hasegawa, "Lowest-ever 0.1419-dB/km loss optical fiber," in *Optical Fiber Communication Conference* (2017), paper Th5D-1.

9. M. Tse, H. Yu, N. Kijbunchoo, *et al.*, "Quantum-enhanced advanced LIGO detectors in the era of gravitational-wave astronomy," Phys. Rev. Lett. **123**, 231107 (2019).

10. A. Buikema, C. Cahillane, G. Mansell, *et al.*, "Sensitivity and performance of the Advanced LIGO detectors in the third observing run," Phys. Rev. D **102**, 062003 (2020).

11. X. Zheng, J. Dolde, V. Lochab, B. N. Merriman, H. Li, and S. Kolkowitz, "High precision differential clock comparisons with a multiplexed optical lattice clock," Nature **602**, 425–430 (2022).

12. T. Bothwell, C. J. Kennedy, A. Aeppli, D. Kedar, J. M. Robinson, E. Oelker, A. Staron, and J. Ye, "Resolving the gravitational redshift within a millimeter atomic sample," Nature **602**, 420–424 (2022).

13. V. B. Braginsky, M. L. Gorodetsky, F. Y. Khalili, and K. S. Thorne, "Energetic quantum limit in large-scale interferometers," AIP Conf. Proc. **523**, 180 (2000).

14. S. D. Bartlett, T. Rudolph, and R. W. Spekkens, "Reference frames, superselection rules, and quantum information," Rev. Mod. Phys. **79**, 555–609 (2007).

15. A. F. Brooks, G. Vajente, H. Yamamoto, *et al.*, "Point absorbers in Advanced LIGO," Appl. Opt. **60**, 4047–4063 (2021).

16. Y. Tamura, H. Sakuma, K. Morita, M. Suzuki, Y. Yamamoto, K. Shimada, Y. Honma, K. Sohma, T. Fujii, and T. Hasegawa, "The first 0.14-dB/km loss optical fiber and its impact on submarine transmission," J. Lightwave Technol. **36**, 44–49 (2018).

17. G. T. Jasion, H. Sakr, J. R. Hayes, S. R. Sandoghchi, L. Hooper, E. N. Fokoua, A. Saljoghei, H. C. Mulvad, M. Alonso, A. Taranta, T. D. Bradley, I. A. Davidson, Y. Chen, D. J. Richardson, and F. Poletti, "0.174 dB/km hollow core double nested antiresonant nodeless fiber (DNANF)," in *Optical Fiber Communications Conference and Exhibition (OFC)* (2022), pp. 1–3.

18. D. Keck, R. Maurer, and P. Schultz, "On the ultimate lower limit of attenuation in glass optical waveguides," Appl. Phys. Lett. **22**, 307–309 (1973).

19. T. Miya, Y. Terunuma, T. Hosaka, and T. Miyashita, "Ultimate low-loss single-mode fibre at 1.55 μm," Electron. Lett. **15**, 106–108 (1979).

20. H. Kanamori, H. Yokota, G. Tanaka, M. Watanabe, Y. Ishiguro, I. Yoshida, T. Kakii, S. Itoh, Y. Asano, and S. Tanaka, "Transmission characteristics and reliability of pure-silica-core single-mode fibers," J. Lightwave Technol. **4**, 1144–1150 (1986).

21. K. Nagayama, M. Kakui, M. Matsui, T. Saitoh, and Y. Chigusa, "Ultra-low-loss (0.1484 dB/km) pure silica core fibre and extension of transmission distance," Electron. Lett. **38**, 1168–1169 (2002).

22. M. Hirano, T. Haruna, Y. Tamura, T. Kawano, S. Ohnuki, Y. Yamamoto, Y. Koyano, and T. Sasaki, "Record low loss, record high FOM optical fiber with manufacturable process," in *Optical Fiber Communication Conference/National Fiber Optic Engineers Conference* (Optica Publishing Group, 2013), paper PDP5A.7.

23. S. Makovejs, C. C. Roberts, F. Palacios, H. B. Matthews, D. A. Lewis, D. T. Smith, P. G. Diehl, J. J. Johnson, J. D. Patterson, C. R. Towery, and S. Y. Ten, "Record-low (0.1460 dB/km) attenuation ultra-large AEFF optical fiber for submarine applications," in *Optical Fiber Communication Conference Post Deadline Papers* (Optica Publishing Group, 2015), paper Th5A.2.

24. B. J. Mangan, L. Farr, A. Langford, P. J. Roberts, D. P. Williams, F. Couny, M. Lawman, M. Mason, S. Coupland, R. Flea, H. Sabert, T. A. Birks, J. C. Knight, and P. St.J. Russell, "Low loss (1.7 dB/km) hollow core photonic bandgap fiber," in *Optical Fiber Communication Conference* (Optica Publishing Group, 2004), paper PD24.

25. P. J. Roberts, F. Couny, H. Sabert, B. J. Mangan, D. P. Williams, L. Farr, M. W. Mason, A. Tomlinson, T. A. Birks, J. C. Knight, and P. St. J. Russell, "Ultimate low loss of hollow-core photonic crystal fibres," Opt. Express **13**, 236–244 (2005).

26. T. D. Bradley, G. T. Jasion, J. R. Hayes, Y. Chen, L. Hooper, H. Sakr, M. Alonso, A. Taranta, A. Saljoghei, H. C. Mulvad, M. Fake, I. A. K. Davidson, N. V. Wheeler, E. N. Fokoua, W. Wang, S. R. Sandoghchi, D. J. Richardson, and F. Poletti, "Antiresonant hollow core fibre with 0.65 dB/km attenuation across the c and l telecommunication bands," in *45th European Conference on Optical Communication (ECOC)* (2019), pp. 1–4.

27. G. T. Jasion, T. D. Bradley, K. Harrington, H. Sakr, Y. Chen, E. N. Fokoua, I. A. Davidson, A. Taranta, J. R. Hayes, D. J. Richardson, and F. Poletti, "Hollow core NANF with 0.28 dB/km attenuation in the C and L bands," in *Optical Fiber Communication Conference Postdeadline Papers* (Optica Publishing Group, 2020), paper Th4B.4.

28. T. Giallorenzi, J. Bucaro, A. Dandridge, G. Sigel, J. Cole, S. Rashleigh, and R. Priest, "Optical fiber sensor technology," IEEE J. Quantum Electron. **18**, 626–665 (1982).

29. S. K. Sheem, T. G. Giallorenzi, and K. Koo, "Optical techniques to solve the signal fading problem in fiber interferometers," Appl. Opt. **21**, 689–693 (1982).

30. K. P. Koo, A. B. Tveten, and A. Dandridge, "Passive stabilization scheme for fiber interferometers using (3×3) fiber directional couplers," Appl. Phys. Lett. **41**, 616–618 (1982).

31. D. A. Jackson, R. Priest, A. Dandridge, and A. B. Tveten, "Elimination of drift in a single-mode optical fiber interferometer using a piezoelectrically stretched coiled fiber," Appl. Opt. **19**, 2926–2929 (1980).

32. A. Dandridge, A. Tveten, and T. Giallorenzi, "Homodyne demodulation scheme for fiber optic sensors using phase generated carrier," IEEE J. Quantum Electron. **18**, 1647–1653 (1982).

33. J. H. Cole, B. A. Danver, and J. A. Bucaro, "Synthetic-heterodyne interferometric demodulation," IEEE Trans. Microw. Theory Tech. **30**, 540–543 (1982).

34. M. A. Nokes, B. C. Hill, and A. E. Barelli, "Fiber optic heterodyne interferometer for vibration measurements in biological systems," Rev. Sci. Instrum. **49**, 722–728 (1978).

35. A. Dandridge, *Fiber Optic Sensors*, 2nd ed. (Wiley, 2011).

36. H. P. Yuen and V. W. Chan, "Noise in homodyne and heterodyne detection," Opt. Lett. **8**, 177–179 (1983).

37. J. Shapiro and S. Wagner, "Phase and amplitude uncertainties in heterodyne detection," IEEE J. Quantum Electron. **20**, 803–813 (1984).

38. M. Nakazawa, "Rayleigh backscattering theory for single-mode optical fibers," J. Opt. Soc. Am. **73**, 1175–1180 (1983).

39. P. Gysel and R. Staubli, "Statistical properties of Rayleigh backscattering in single-mode fibers," J. Lightwave Technol. **8**, 561–567 (1990).

40. S. Wu, A. Yariv, H. Blauvelt, and N. Kwong, "Theoretical and experimental investigation of conversion of phase noise to intensity noise by Rayleigh scattering in optical fibers," Appl. Phys. Lett. **59**, 1156 (1991).

41. P. Wan and J. Conradi, "Impact of double Rayleigh backscatter noise on digital and analog fiber systems," J. Lightwave Technol. **14**, 288–297 (1996).

42. M. O. van Deventer, "Polarization properties of Rayleigh backscattering in single-mode fibers," J. Lightwave Technol. **11**, 1895–1899 (1993).

43. M. Fleyer, S. Heerschap, G. A. Cranch, and M. Horowitz, "Noise induced in optical fibers by double Rayleigh scattering of a laser with a $1/f^\nu$ frequency noise," Opt. Lett. **41**, 1265–1268 (2016).

44. G. Cranch, A. Dandridge, and C. Kirkendall, "Suppression of double Rayleigh scattering-induced excess noise in remotely interrogated fiber-optic interferometric sensors," IEEE Photon. Technol. Lett. **15**, 1582–1584 (2003).

45. W. H. Glenn, "Noise in interferometric optical systems: an optical Nyquist theorem," IEEE J. Quantum Electron. **25**, 1218–1224 (1989).

46. K. H. Wanser, "Fundamental phase noise limit in optical fibres due to temperature fluctuations," Electron. Lett. **28**, 53–54 (1992).

47. S. Foster, A. Tikhomirov, and M. Milnes, "Fundamental thermal noise in distributed feedback fiber lasers," IEEE J. Quantum Electron. **43**, 378–384 (2007).

48. L. Duan, "General treatment of the thermal noises in optical fibers," Phys. Rev. A **86**, 023817 (2012).

49. R. E. Bartolo, A. B. Tveten, and A. Dandridge, "Thermal phase noise measurements in optical fiber interferometers," IEEE J. Quantum Electron. **48**, 720–727 (2012).

50. H. Callen and T. Welton, "Irreversibility and generalized noise," Phys. Rev. **83**, 34 (1951).

51. R. Kubo, "The fluctuation-dissipation theorem," Rep. Prog. Phys. **29**, 255 (1966).

52. Y. Levin, "Internal thermal noise in the LIGO test masses: a direct approach," Phys. Rev. D **57**, 659–663 (1998).

53. L. Duan, "Intrinsic thermal noise of optical fibres due to mechanical dissipation," Electron. Lett. **46**, 1515–1516 (2010).

54. P. R. Saulson, "Thermal noise in mechanical experiments," Phys. Rev. D **42**, 2437–2445 (1990).

55. J. Dong, J. Huang, T. Li, and L. Liu, "Observation of fundamental thermal noise in optical fibers down to infrasonic frequencies," Appl. Phys. Lett. **108**, 021108 (2016).

56. R. M. Shelby, M. D. Levenson, and P. W. Bayer, "Resolved forward Brillouin scattering in optical fibers," Phys. Rev. Lett. **54**, 939–942 (1985).

57. R. M. Shelby, M. D. Levenson, and P. W. Bayer, "Guided acoustic-wave Brillouin scattering," Phys. Rev. B **31**, 5244–5252 (1985).

58. M. Yoshida, N. Takefushi, K. Kasai, T. Hirooka, and M. Nakazawa, "Precise measurements and their analysis of GAWBS-induced depolarization noise in various optical fibers for digital coherent transmission," Opt. Express **28**, 34422–34433 (2020).

59. V. Sudhir, *Quantum Limits on Measurement and Control of a Mechanical Oscillator*, 1st ed. (Springer International Publishing, 2018).

60. G. I. González and P. R. Saulson, "Brownian motion of a torsion pendulum with internal friction," Phys. Lett. A **201**, 12–18 (1995).

61. N. Takefushi, M. Yoshida, K. Kasai, T. Hirooka, and M. Nakazawa, "Theoretical and experimental analyses of GAWBS phase noise in various optical fibers for digital coherent transmission," Opt. Express **28**, 2873–2883 (2020).

62. A. J. Poustie, "Bandwidth and mode intensities of guided acoustic-wave Brillouin scattering in optical fibers," J. Opt. Soc. Am. B **10**, 691–696 (1993).

63. A. J. Poustie, "Guided acoustic-wave Brillouin scattering with optical pulses," Opt. Lett. **17**, 574–576 (1992).

64. M. Johnson, "Poincaré sphere representation of birefringent networks," Appl. Opt. **20**, 2075–2080 (1981).

65. A. D. Kersey, A. Dandridge, and A. B. Tveten, "Dependence of visibility on input polarization in interferometric fiber-optic sensors," Opt. Lett. **13**, 288–290 (1988).

66. G. D. VanWiggeren and R. Roy, "Transmission of linearly polarized light through a single-mode fiber with random fluctuations of birefringence," Appl. Opt. **38**, 3888–3892 (1999).

67. J. P. Gordon and H. Kogelnik, "PMD fundamentals: polarization mode dispersion in optical fibers," Proc. Natl. Acad. Sci. USA **97**, 4541–4550 (2000).

68. C. D. Poole and R. E. Wagner, "Phenomenological approach to polarisation dispersion in long single-mode fibres," Electron. Lett. **22**, 1029–1030 (1986).

69. A. D. Kersey, M. J. Marrone, and A. Dandridge, "Observation of input-polarization-induced phase noise in interferometric fiber-optic sensors," Opt. Lett. **13**, 847–849 (1988).

70. A. D. Kersey, M. J. Marrone, and A. Dandridge, "Analysis of input-polarization-induced phase noise in interferometric fiber-optic sensors and its reduction using polarization scrambling," J. Lightwave Technol. **8**, 838–845 (1990).

71. C. K. Kirkendall and A. Dandridge, "Overview of high performance fibre-optic sensing," J. Phys. D **37**, R197 (2004).

72. N. J. Frigo, A. Dandridge, and A. B. Tveten, "Technique for elimination of polarisation fading in fibre interferometers," Electron. Lett. **20**, 319–320 (1984).

73. K. H. Wanser and N. H. Safar, "Remote polarization control for fiber-optic interferometers," Opt. Lett. **12**, 217–219 (1987).

74. A. D. Kersey, M. J. Marrone, A. Dandridge, and A. B. Tveten, "Optimization and stabilization of visibility in interferometric fiber-optic sensors using input-polarization control," J. Lightwave Technol. **6**, 1599–1609 (1988).

75. M. Martinelli, "A universal compensator for polarization changes induced by birefringence on a retracing beam," Opt. Commun. **72**, 341–344 (1989).

76. S. Kryhin, E. D. Hall, and V. Sudhir, "Thermorefringent noise in crystalline optical materials," arXiv:2111.05433 (2021).

77. G. Agrawal, *Nonlinear Fiber Optics*, 5th ed. (Academic, 2013).

78. S. Evangelides, L. Mollenauer, J. Gordon, and N. Bergano, "Polarization multiplexing with solitons," J. Lightwave Technol. **10**, 28–35 (1992).

79. P. Wai and C. Menyak, "Polarization mode dispersion, decorrelation, and diffusion in optical fibers with randomly varying birefringence," J. Lightwave Technol. **14**, 148–157 (1996).

80. R. Dar, M. Feder, A. Mecozzi, and M. Shtaif, "Properties of nonlinear noise in long, dispersion-uncompensated fiber links," Opt. Express **21**, 25685–25699 (2013).

81. R. Dar, M. Feder, A. Mecozzi, and M. Shtaif, "Accumulation of nonlinear interference noise in fiber-optic systems," Opt. Express **22**, 14199–14211 (2014).

82. P. Poggiolini, "The GN model of non-linear propagation in uncompensated coherent optical systems," J. Lightwave Technol. **30**, 3857–3879 (2012).

83. A. Carena, G. Bosco, V. Curri, Y. Jiang, P. Poggiolini, and F. Forghieri, "EGN model of non-linear fiber propagation," Opt. Express **22**, 16335–16362 (2014).

84. R. W. Tkach, A. R. Chraplyvy, F. Forghieri, A. H. Gnauck, and R. M. Derosier, "Four-photon mixing and high-speed WDM systems," J. Lightwave Technol. **13**, 841–849 (1995).

85. K. O. Hill, D. C. Johnson, B. S. Kawasaki, and R. I. MacDonald, "CW three-wave mixing in single-mode optical fibers," J. Appl. Phys. **49**, 5098–5106 (1978).

86. N. Shibata, R. Braun, and R. Waarts, "Phase-mismatch dependence of efficiency of wave generation through four-wave mixing in a single-mode optical fiber," IEEE J. Quantum Electron. **23**, 1205–1210 (1987).

87. K. Inoue, "Phase-mismatching characteristic of four-wave mixing in fiber lines with multistage optical amplifiers," Opt. Lett. **17**, 801–803 (1992).

88. J. A. Buck, *Fundamentals of Optical Fibers*, 2nd ed. (Wiley, 2004).

89. A. Kobyakov, M. Sauer, and D. Chowdhury, "Stimulated Brillouin scattering in optical fibers," Adv. Opt. Photon. **2**, 1–59 (2010).

90. R. G. Smith, "Optical power handling capacity of low loss optical fibers as determined by stimulated Raman and Brillouin scattering," Appl. Opt. **11**, 2489–2494 (1972).

91. A. B. Ruffin, M.-J. Li, X. Chen, A. Kobyakov, and F. Annunziata, "Brillouin gain analysis for fibers with different refractive indices," Opt. Lett. **30**, 3123–3125 (2005).

92. A. P. Kung, A. Agarwal, D. F. Grosz, S. Banerjee, and D. N. Maywar, "Analytical solution of transmission performance improvement in fiber spans with forward Raman gain and its application to repeaterless systems," J. Lightwave Technol. **23**, 1182–1188 (2005).

93. M. O. van Deventer and A. J. Boot, "Polarization properties of stimulated Brillouin scattering in single-mode fibers," J. Lightwave Technol. **12**, 585–590 (1994).

94. A. B. Ruffin, "Stimulated Brillouin scattering: an overview of measurements, system impairments, and applications," in *Technical Digest: Symposium on Optical Fiber Measurements* (2004), pp. 23–28.

95. A. Kobyakov, S. Kumar, D. Q. Chowdhury, A. B. Ruffin, M. Sauer, S. R. Bickham, and R. Mishra, "Design concept for optical fibers with enhanced SBS threshold," Opt. Express **13**, 5338–5346 (2005).

96. R. H. Stolen, C. Lee, and R. K. Jain, "Development of the stimulated Raman spectrum in single-mode silica fibers," J. Opt. Soc. Am. B **1**, 652–657 (1984).

97. M. Ahmed and M. Yamada, "Effect of intensity noise of semiconductor lasers on the digital modulation characteristics and the bit error rate of optical communication systems," J. Appl. Phys. **104**, 013104 (2008).

98. D. P. Blair and P. H. Sydenham, "Phase sensitive detection as a means to recover signals buried in noise," J. Phys. E **8**, 621–627 (1975).

99. D. S. Elliott, R. Roy, and S. J. Smith, "Extracavity laser band-shape and bandwidth modification," Phys. Rev. A **26**, 12–18 (1982).

100. G. D. Domenico, S. Schilt, and P. Thomann, "Simple approach to the relation between laser frequency noise and laser line shape," Appl. Opt. **49**, 4801–4807 (2010).

101. J. A. Armstrong, "Theory of interferometric analysis of laser phase noise*," J. Opt. Soc. Am. **56**, 1024–1031 (1966).

102. P. Gallion and G. Debarge, "Quantum phase noise and field correlation in single frequency semiconductor laser systems," IEEE J. Quantum Electron. **20**, 343–349 (1984).

103. F. Kéfélian, H. Jiang, P. Lemonde, and G. Santarelli, "Ultralow-frequency-noise stabilization of a laser by locking to an optical fiber-delay line," Opt. Lett. **34**, 914–916 (2009).

104. K. Aki and P. G. Richards, *Quantitative Seismology* (University Science Books, 2009).

105. F. Ardhuin, E. Stutzmann, M. Schimmel, and A. Mangeney, "Ocean wave sources of seismic noise," J. Geophys. Res. Oceans **116**, C006952 (2011).

106. N. Nakata, L. Gualtieri, and A. Fichtner, *Seismic Ambient Noise* (Cambridge University, 2019).

107. D. E. McNamara and R. P. Buland, "Ambient noise levels in the continental united states," Bull. Seismol. Soc. Am. **94**(4), 1517–1527 (2004).

108. K. Hasselmann, "A statistical analysis of the generation of microseisms," Rev. Geophys. **1**, 177–210 (1963).

109. L. Gualtieri, E. Bachmann, F. J. Simons, and J. Tromp, "The origin of secondary microseism Love waves," Proc. Natl. Acad. Sci. USA **117**, 29504–29511 (2020).

110. S. C. Webb, "The Earth's 'hum' is driven by ocean waves over the continental shelves," Nature **445**, 754–756 (2007).

111. W. L. Down, "Natural infrasound of five seconds period," Nature **215**, 1469–1470 (1967).

112. W. L. Donn and B. Naini, "Sea wave origin of microbaroms and microseisms," J. Geophys. Res. **78**, 4482–4488 (1973).

113. G. B. Hocker, "Fiber-optic sensing of pressure and temperature," Appl. Opt. **18**, 1445–1448 (1979).

114. N. Ashby, D. A. Howe, J. Taylor, A. Hati, and C. Nelson, "Optical fiber vibration and acceleration model," in *IEEE International Frequency Control Symposium Joint with the 21st European Frequency and Time Forum* (2007), pp. 547–551.

115. M. A. Zumberge, J. Berger, M. A. H. Hedlin, E. Husmann, S. Nooner, R. Hilt, and R. Widmer-Schnidrig, "An optical fiber infrasound sensor: a new lower limit on atmospheric pressure noise between 1 and 10 Hz," J. Acoust. Soc. Am. **113**, 2474–2479 (2003).

116. J. C. V. Minář, H. de Riedmatten, C. Simon, H. Zbinden, and N. Gisin, "Phase-noise measurements in long-fiber interferometers for quantum-repeater applications," Phys. Rev. A **77**, 052325 (2008).

117. J. Harms, "Terrestrial gravity fluctuations," Living Rev. Relativ. **22**, 1–154 (2019).

118. S. A. Hughes and K. S. Thorne, "Seismic gravity-gradient noise in interferometric gravitational-wave detectors," Phys. Rev. D **58**, 122002 (1998).

119. T. Creighton, "Tumbleweeds and airborne gravitational noise sources for LIGO," Class. Quantum Gravity **25**, 125011 (2008).

120. P. St.J. Russell, "Photonic crystal fibers," Science **299**, 358–362 (2003).

121. J. Broeng, D. Mogilevstev, S. E. Barkou, and A. Bjarklev, "Photonic crystal fibers: a new class of optical waveguides," Opt. Fiber Technol. **5**, 305–330 (1999).

122. E. Yablonovitch, "Photonic band-gap structures," J. Opt. Soc. Am. B **10**, 283–295 (1993).

123. T. Birks, P. Roberts, P. St.J. Russell, D. Atkin, and T. Shepherd, "Full 2-D photonic bandgaps in silica/air structures," Electron. Lett. **31**, 1941–1943 (1995).

124. R. F. Cregan, B. J. Mangan, J. C. Knight, T. A. Birks, P. St.J. Russell, P. J. Roberts, and D. C. Allan, "Single-mode photonic band gap guidance of light in air," Science **285**, 1537–1539 (1999).

125. M. A. Duguay, Y. Kokubun, T. L. Koch, and L. Pfeiffer, "Antiresonant reflecting optical waveguides in SiO_2-Si multilayer structures," Appl. Phys. Lett. **49**, 13–15 (1986).

126. T. A. Birks, J. C. Knight, and P. St.J. Russell, "Endlessly single-mode photonic crystal fiber," Opt. Lett. **22**, 961–963 (1997).

127. J. C. Knight, T. A. Birks, R. F. Cregan, and P. St.J. Russell, "Large mode area photonic crystal fiber," Opt. Photon. News **9**(12), 34–35 (1998).

128. T. Birks, D. Mogilevtsev, J. Knight, and P. St.J. Russell, "Dispersion compensation using single-material fibers," IEEE Photon. Technol. Lett. **11**, 674–676 (1999).

129. P. Yeh, A. Yariv, and E. Marom, "Theory of Bragg fiber*," J. Opt. Soc. Am. **68**, 1196–1201 (1978).

130. S. G. Johnson, M. Ibanescu, M. Skorobogatiy, O. Weisberg, T. D. Engeness, M. Soljačić, S. A. Jacobs, J. D. Joannopoulos, and Y. Fink, "Low-loss asymptotically single-mode propagation in large-core omniguide fibers," Opt. Express **9**, 748–779 (2001).

131. F. Poletti, M. N. Petrovich, and D. J. Richardson, "Hollow-core photonic bandgap fibers: technology and applications," Nanophotonics **2**, 315–340 (2013).

132. F. Couny, F. Benabid, and P. S. Light, "Large-pitch Kagome-structured hollow-core photonic crystal fiber," Opt. Lett. **31**, 3574–3576 (2006).

133. C. Wei, R. Joseph Weiblen, C. R. Menyuk, and J. Hu, "Negative curvature fibers," Adv. Opt. Photon. **9**, 504–561 (2017).

134. V. Dangui, M. J. F. Digonnet, and G. S. Kino, "Modeling of the propagation loss and backscattering in air-core photonic-bandgap fibers," J. Lightwave Technol. **27**, 3783–3789 (2009).

135. V. Michaud-Belleau, E. Numkam Fokoua, T. D. Bradley, J. R. Hayes, Y. Chen, F. Poletti, D. J. Richardson, J. Genest, and R. Slavík, "Backscattering in antiresonant hollow-core fibers: over 40 dB lower than in standard optical fibers," Optica **8**, 216–219 (2021).

136. E. Numkam Fokoua, V. Michaud-Belleau, J. Genest, R. Slavík, and F. Poletti, "Theoretical analysis of backscattering in hollow-core antiresonant fibers," APL Photon. **6**, 096106 (2021).

137. F. Poletti, "Nested antiresonant nodeless hollow core fiber," Opt. Express **22**, 23807–23828 (2014).

138. G. A. Sanders, A. A. Taranta, C. Narayanan, E. Numkam Fokoua, S. Abokhamis Mousavi, L. K. Strandjord, M. Smiciklas, T. D. Bradley, J. Hayes, G. T. Jasion, T. Qiu, W. Williams, F. Poletti, and D. N. Payne, "Hollow-core resonator fiber optic gyroscope using nodeless anti-resonant fiber," Opt. Lett. **46**, 46–49 (2021).

139. R. Slavík, E. R. N. Fokoua, M. Bukshtab, Y. Chen, T. D. Bradley, S. R. Sandoghchi, M. N. Petrovich, F. Poletti, and D. J. Richardson, "Demonstration of opposing thermal sensitivities in hollow-core fibers with open and sealed ends," Opt. Lett. **44**, 4367–4370 (2019).

140. V. Dangui, H. K. Kim, M. J. F. Digonnet, and G. S. Kino, "Phase sensitivity to temperature of the fundamental mode in air-guiding photonic-bandgap fibers," Opt. Express **13**, 6669–6684 (2005).

141. R. Slavík, G. Marra, E. N. Fokoua, N. Baddela, N. V. Wheeler, M. Petrovich, F. Poletti, and D. J. Richardson, "Ultralow thermal sensitivity of phase and propagation delay in hollow core optical fibres," Sci. Rep. **5**, 15447 (2015).

142. S. Meiselman and G. A. Cranch, "Optical phase response to temperature in a hollow-core photonic crystal fiber," Opt. Express **25**, 27581–27594 (2017).

143. W. Zhu, E. R. N. Fokoua, Y. Chen, T. Bradley, M. N. Petrovich, F. Poletti, M. Zhao, D. J. Richardson, and R. Slavík, "Temperature insensitive fiber interferometry," Opt. Lett. **44**, 2768–2770 (2019).

144. W. Zhu, E. R. Numkam Fokoua, A. A. Taranta, Y. Chen, T. Bradley, M. N. Petrovich, F. Poletti, M. Zhao, D. J. Richardson, and R. Slavík, "The thermal phase sensitivity of both coated and uncoated standard and hollow core fibers down to cryogenic temperatures," J. Lightwave Technol. **38**, 2477–2484 (2020).

145. B. Merkel, D. Repp, and A. Reiserer, "Laser stabilization to a cryogenic fiber ring resonator," Opt. Lett. **46**, 444–447 (2021).

146. B. Shi, H. Sakr, J. Hayes, X. Wei, E. N. Fokoua, M. Ding, Z. Feng, G. Marra, F. Poletti, D. J. Richardson, and R. Slavík, "Thinly coated hollow core fiber for improved thermal phase-stability performance," Opt. Lett. **46**, 5177–5180 (2021).

147. P. Ma, N. Song, J. Jin, J. Song, and X. Xu, "Birefringence sensitivity to temperature of polarization maintaining photonic crystal fibers," Opt. Laser Technol. **44**, 1829–1833 (2012).

148. G. A. Cranch and G. A. Miller, "Coherent light transmission properties of commercial photonic crystal hollow core optical fiber," Appl. Opt. **54**, F8–F16 (2015).

149. V. Michaud-Belleau, E. R. Numkam Fokoua, P. Horak, N. V. Wheeler, S. Rikimi, T. D. Bradley, D. J. Richardson, F. Poletti, J. Genest, and R. Slavík, "Fundamental thermal noise in antiresonant hollow-core fibers," Phys. Rev. A **106**, 023501 (2022).

150. V. Laude, A. Khelif, S. Benchabane, M. Wilm, T. Sylvestre, A. Mussot, J. M. Dudley, and H. Maillotte, "Phononic band-gap guidance of acoustic modes in photonic crystal fibers," Phys. Rev. B **71**, 045107 (2005).

151. D. Elser, U. L. Andersen, A. Korn, O. Glöckl, S. Lorenz, C. Marquardt, and G. Leuchs, "Reduction of guided acoustic wave Brillouin scattering in photonic crystal fibers," Phys. Rev. Lett. **97**, 133901 (2006).

152. J.-C. Beugnot, T. Sylvestre, H. Maillotte, G. Mélin, and V. Laude, "Guided acoustic wave Brillouin scattering in photonic crystal fibers," Opt. Lett. **32**, 17–19 (2007).

153. M. S. Kang, A. Nazarkin, A. Brenn, and P. St.J. Russell, "Tightly trapped acoustic phonons in photonic crystal fibres as highly nonlinear artificial Raman oscillators," Nat. Phys. **5**, 276–280 (2009).

154. B. Stiller, M. Delqué, J.-C. Beugnot, M. W. Lee, G. Mélin, H. Maillotte, V. Laude, and T. Sylvestre, "Frequency-selective excitation of guided acoustic modes in a photonic crystal fiber," Opt. Express **19**, 7689–7694 (2011).

155. P. F. Jarschel, E. Lamilla, Y. A. V. Espinel, I. Aldaya, J. L. Pita, A. Gil-Molina, G. S. Wiederhecker, and P. Dainese, "Intermodal Brillouin scattering in solid-core photonic crystal fibers," APL Photon. **6**, 036108 (2021).

156. W. E. née Zhong, B. Stiller, D. Elser, B. Heim, C. Marquardt, and G. Leuchs, "Depolarized guided acoustic wave Brillouin scattering in hollow-core photonic crystal fibers," Opt. Express **23**, 27707–27714 (2015).

157. W. H. Renninger, R. O. Behunin, and P. T. Rakich, "Guided-wave Brillouin scattering in air," Optica **3**, 1316–1319 (2016).

158. W. H. Renninger, H. Shin, R. O. Behunin, P. Kharel, E. A. Kittlaus, and P. T. Rakich, "Forward Brillouin scattering in hollow-core photonic bandgap fibers," New J. Phys. **18**, 025008 (2016).

159. A. Iyer, W. Xu, J. E. Antonio-Lopez, R. A. Correa, and W. H. Renninger, "Ultra-low Brillouin scattering in anti-resonant hollow-core fibers," APL Photon. **5**, 096109 (2020).

160. F. Poletti, N. G. R. Broderick, D. J. Richardson, and T. M. Monro, "The effect of core asymmetries on the polarization properties of hollow core photonic bandgap fibers," Opt. Express **13**, 9115–9124 (2005).

161. G. Bouwmans, F. Luan, J. C. Knight, P. St.J. Russell, L. Farr, B. J. Mangan, and H. Sabert, "Properties of a hollow-core photonic bandgap fiber at 850 nm wavelength," Opt. Express **11**, 1613–1620 (2003).

162. J. M. Fini, J. W. Nicholson, B. Mangan, L. Meng, R. S. Windeler, E. M. Monberg, A. DeSantolo, F. V. DiMarcello, and K. Mukasa, "Polarization maintaining single-mode low-loss hollow-core fibres," Nat. Commun. **5**, 5085 (2014).

163. A. Taranta, E. Numkam Fokoua, S. Abokhamis Mousavi, J. R. Hayes, T. D. Bradley, G. T. Jasion, and F. Poletti, "Exceptional polarization purity in antiresonant hollow-core optical fibres," Nat. Photonics **14**, 504–510 (2020).

164. N. G. R. Broderick, T. M. Monro, P. J. Bennett, and D. J. Richardson, "Nonlinearity in holey optical fibers: measurement and future opportunities," Opt. Lett. **24**, 1395–1397 (1999).

165. J. M. Dudley and J. R. Taylor, "Ten years of nonlinear optics in photonic crystal fibre," Nat. Photonics **3**, 85–90 (2009).

166. A. R. Bhagwat and A. L. Gaeta, "Nonlinear optics in hollow-core photonic bandgap fibers," Opt. Express **16**, 5035–5047 (2008).

167. F. Yang, F. Gyger, and L. Thévenaz, "Intense Brillouin amplification in gas using hollow-core waveguides," Nat. Photonics **14**, 700–708 (2020).

168. J. R. Peterson, "Observations and modeling of seismic background noise," USGS Numbered Series 93-322 (U.S. Geological Survey, 1993).

169. J. Berger, P. Davis, and G. Ekstrom, "Ambient Earth noise: a survey of the global seismographic network," J. Geophys. Res. Solid Earth **109**, B11307 (2004).

170. P. A. Williams, W. C. Swann, and N. R. Newbury, "High-stability transfer of an optical frequency over long fiber-optic links," J. Opt. Soc. Am. B **25**, 1284–1293 (2008).

171. P. Linsay, P. Saulson, and R. Weiss, "A study of a long baseline gravitational wave antenna system," LIGO Document T830001-x0 (1983).

172. K. Tanaka, "How to detect the gravitationally induced phase shift of electromagnetic waves by optical-fiber interferometry," Phys. Rev. Lett. **51**, 378–380 (1983).

173. M. Zych, F. Costa, I. Pikovski, T. C. Ralph, and C. Brukner, "General relativistic effects in quantum interference of photons," Class. Quantum Gravity **29**, 224010 (2012).

174. D. Rideout, T. Jennewein, G. Amelino-Camelia, et al., "Fundamental quantum optics experiments conceivable with satellites–reaching relativistic distances and velocities," Class. Quantum Gravity **29**, 224011 (2012).

175. C. Hilweg, F. Massa, D. Martynov, N. Mavalvala, P. T. Chruściel, and P. Walther, "Gravitationally induced phase shift on a single photon," New J. Phys. **19**, 033028 (2017).

176. S. Pallister, S. Coop, V. Formichella, N. Gampierakis, V. Notaro, P. Knott, R. Azevedo, N. Buchheim, S. de Carvalho, E. Järvelä, M. Laporte, J.-P. Kaikkonen, N. Meshksar, T. Nikkanen, and M. Yttergren, "A blueprint for a simultaneous test of quantum mechanics and general relativity in a space-based quantum optics experiment," EPJ Quantum Technol. **4**, 2 (2017).

177. M. Rivera-Tapia, M. I. Yáñez Reyes, A. Delgado, and G. Rubilar, "Outperforming classical estimation of post-Newtonian parameters of Earth's gravitational field using quantum metrology," arxiv:2101.12126 (2021).

178. L. Esmaeilifar and T. C. Ralph, "Gravitational acceleration estimation with a nonlinear Mach–Zehnder interferometer," J. Opt. Soc. Am. B **39**, 421–426 (2022).

179. S. Droste, F. Ozimek, T. Udem, K. Predehl, T. W. Hänsch, H. Schnatz, G. Grosche, and R. Holzwarth, "Optical-frequency transfer over a single-span 1840 km fiber link," Phys. Rev. Lett. **111**, 110801 (2013).

180. S. Droste, T. Udem, R. Holzwarth, and T. W. Hänsch, "Optical frequency dissemination for metrology applications," C.R. Phys. **16**, 524–530 (2015), the measurement of time/La mesure du temps.

181. S. M. F. Raupach, A. Koczwara, and G. Grosche, "Brillouin amplification supports 1×10^{-20} uncertainty in optical frequency transfer over 1400 km of underground fiber," Phys. Rev. A **92**, 021801 (2015).

182. F. Riehle, "Optical clock networks," Nat. Photonics **11**, 25–31 (2017).

183. L. Hu, X. Tian, G. Wu, M. Kong, J. Shen, and J. Chen, "Multi-node optical frequency dissemination with post automatic phase correction," J. Lightwave Technol. **38**, 3644–3651 (2020).

184. J. Grotti, S. Koller, S. Vogt, et al., "Geodesy and metrology with a transportable optical clock," Nat. Phys. **14**, 437–441 (2018).

185. M. Schioppo, J. Kronjäger, A. Silva, et al., "Comparing ultrastable lasers at 7×10^{-17} fractional frequency instability through a 2220 km optical fibre network," Nat. Commun. **13**, 212 (2022).

186. N. Gisin and R. Thew, "Quantum communication," Nat. Photonics **1**, 165–171 (2007).

187. J.-P. Chen, C. Zhang, Y. Liu, C. Jiang, W.-J. Zhang, Z.-Y. Han, S.-Z. Ma, X.-L. Hu, Y.-H. Li, H. Liu, F. Zhou, H.-F. Jiang, T.-Y. Chen, H. Li, L.-X. You, Z. Wang, X.-B. Wang, Q. Zhang, and J.-W. Pan, "Twin-field quantum key distribution over a 511 km optical fibre linking two distant metropolitan areas," Nat. Photonics **15**, 570–575 (2021).

188. S. Wang, Z.-Q. Yin, D.-Y. He, W. Chen, R.-Q. Wang, P. Ye, Y. Zhou, G.-J. Fan-Yuan, F.-X. Wang, W. Chen, Y.-G. Zhu, P. V. Morozov, A. V. Divochiy, Z. Zhou, G.-C. Guo, and Z.-F. Han, "Twin-field quantum key distribution over 830-km fibre," Nat. Photonics **16**, 154–161 (2022).